GLOBAL BIOGEOCHEMICAL CYCLES, VOL. 12, NO. 2, PAGES 259-276, JUNE 1998

# Dynamics of fossil fuel $CO_2$ neutralization by marine $CaCO_3$

David Archer

Department of the Geophysical Sciences, University of Chicago
Chicago, Illinois

Haroon Kheshgi

Exxon Research and Engineering Company, Annandale, New Jersey

Ernst Maier-Reimer

Max-Plank-Institut für Meteorologie, Hamburg , Germany

**Abstract.** A detailed model of the ocean circulation and carbon cycle was coupled to a mechanistic model of $CaCO_3$ diagenesis in deep sea sediments to simulate the millennium-scale response of the oceans to future fossil fuel $CO_2$ emissions to the atmosphere and deep sea. Simulations of deep sea injection of $CO_2$ show that $CaCO_3$ dissolution is sensitive to passage of high-$CO_2$ waters through the Atlantic Ocean, but $CaCO_3$ dissolution has a negligible impact on atmospheric $pCO_2$ or the atmospheric stabilization $CO_2$ emission in the coming centuries. The ultimate fate of the fossil fuel $CO_2$ will be to react with $CaCO_3$ on the seafloor and on land. An initial $CaCO_3$ dissolution spike reverses the net sedimentation rate in the ocean until it is attenuated by an enhanced vertical gradient of alkalinity after about 1000 years. The magnitude of the initial spike is sensitive to assumptions about the kinetics for $CaCO_3$ dissolution, but subsequent behavior appears to be less model dependent. Neutralization by seafloor $CaCO_3$ occurs on a timescale of 5-6 kyr, and is limited to at most 60-70% of the fossil fuel release, even if the fossil fuel release is smaller than the seafloor erodible inventory of $CaCO_3$. Additional neutralization by terrestrial $CaCO_3$ restores a balance between $CaCO_3$ weathering and seafloor accumulation on a timescale of 8.5 kyr, while the deficit of seafloor $CaCO_3$ (the lysocline) is replenished with an *e*-folding timescale of approximately 18 kyr. The final equilibrium with $CaCO_3$ leaves 7-8% of the fossil fuel $CO_2$ remaining in the atmosphere, to be neutralized by the silicate rock cycle on a time frame of hundreds of thousands of years.

## 1. Introduction

Mankind releases $CO_2$ to the atmosphere by combustion of fossil fuels and by deforestation, which converts relatively high biomass forests, mostly in the tropics, into lower biomass grasslands and farmlands, resulting in a net release of $CO_2$. Currently, the rate of atmospheric $CO_2$ increase corresponds to less than half of the anthropogenic release from fossil fuels and deforestation. The sink for the other half appears to be a combination of dissolution into the ocean and uptake by the terrestrial biosphere in regions other than regions of active deforestation [*Tans et al.*, 1990; *Schimel et al.*, 1994; *Cias et al.*, 1995; *Jain et al.*, 1996; *Keeling et al.*, 1996; *Kheshgi et al.*, 1996]. Future uptake by the terrestrial biosphere is difficult to predict and is not the topic of this paper. In contrast, uptake by the oceans is describable by the physics of ocean circulation and the chemistry of $CO_2$ and $CaCO_3$, which we are beginning to be able to describe quantitatively. For our discussion of the oceanic $CO_2$ uptake, it will be convenient to combine anthropogenic emission and biospheric uptake into a quantity called the net terrestrial emission, such that future biosphere uptake acts to directly counteract fossil fuel and deforestation $CO_2$ emission.

The first and quantitatively most significant step in the processing of the terrestrial $CO_2$ release will be dissolution in the oceans, which we will call invasion. The timescale for invasion is determined by the circulation timescale of the ocean and by the buffer capacity of subducting surface seawater. Following the equilibration of the atmosphere with the water in the ocean, the $CO_2$ will react with solid $CaCO_3$ (a reaction called neutralization), decreasing the atmospheric component of the $CO_2$ release still further. Two processes contribute to neutralization: (1) the transfer of carbonate ion [$CO_3^=$] from dissolving $CaCO_3$ on the seafloor to the ocean (seafloor neutralization) and (2) the imbalance between the rate of chemical weathering (dissolving) of $CaCO_3$ on land and accumulation of solid $CaCO_3$ on the seafloor, which results in a net dissolution flux of $CaCO_3$ on land to the ocean (terrestrial neutralization). Finally, on time frames of hundreds of



Paper number 98GB00744
0886-6236/98/98GB-00744$12.00

thousands of years the $pCO_2$ of the atmosphere (and hence the ocean) is thought to be controlled by the balance between volcanic degassing of $CO_2$ and its consumption by reaction with basic components of silicate rocks [*Walker and Kasting*, 1992].

In this paper, we subject a detailed model of ocean and sediment carbon chemistry to a range of fossil fuel release scenarios to predict the impact of $CaCO_3$ dissolution on time frames of centuries to millennia. Section 2 describes the model in detail. Sections 3 and 4 analyze the effect of $CaCO_3$ on estimates of the net terrestrial emission which result in specified time-evolution of atmospheric $CO_2$ concentration (stabilization scenarios), and results of deep sea $CO_2$ direct injection experiments. Section 5, the longest section, describes the sequence of invasion and seafloor and terrestrial neutralization to the year A.D. 10,000 and beyond in response to various $CO_2$ release scenarios. We explore the dynamics of fossil fuel neutralization to understand the details of the kinetics of neutralization in its various regimes, an understanding which may also guide future research into the transitions in global carbon cycle accompanying the transitions between glacial and interglacial states.

## 2. Model Description

We simulate the physics and chemistry of the ocean and sediment response to anthropogenic $CO_2$ release using a previously documented model of ocean circulation and water column chemistry [*Maier-Reimer*, 1993b], coupled to a sedimentary diagenesis model for organic carbon and $CaCO_3$ in deep sea sediments [*Archer*, 1991, 1996b]. The ocean carbon cycle model advects dissolved chemical tracers using the steady flow field from the large scale geostrophic circulation model, tuned to represent the present-day ocean [*Maier-Reimer*, 1993b]. The model flow field was invariant during the model integration, neglecting climate feedbacks to ocean flow [*Manabe and Stouffer*, 1993]. A single nutrient, scaled to represent $PO_4^{3-}$, limits organic carbon export from the surface ocean according to the Michaelis-Menton rate expression

$$\text{Rate} = r_{\text{lat}} \frac{P^2}{P + P_{\text{HS}}}$$

where $r_{\text{lat}}$ is a function of latitude (light) and temperature, $P$ is the nutrient concentration, and $P_{\text{HS}}$ is the half-saturation constant, set at a value of 0.01 μmol $L^{-1}$. This production rate has been adjusted relative to the formulation of *Maier-Reimer*[1993b] to slow the biological uptake of nutrients in the euphotic zone, decreasing the rate of biological productivity in high-nutrient areas such as the equatorial Pacific, allowing transport of nutrients in surface currents to the oligotropic subtropical gyres. This was necessary to attenuate the equator/oligotrophic contrast in the delivery rates of organic carbon and $CaCO_3$ to the seafloor. The resulting export productivity field of the ocean is shown in Plate 1a. The disadvantage of this adjustment was an increase in the nutrient concentration and $pCO_2$ of the sea surface, increasing the $pCO_2$ of the model atmosphere by

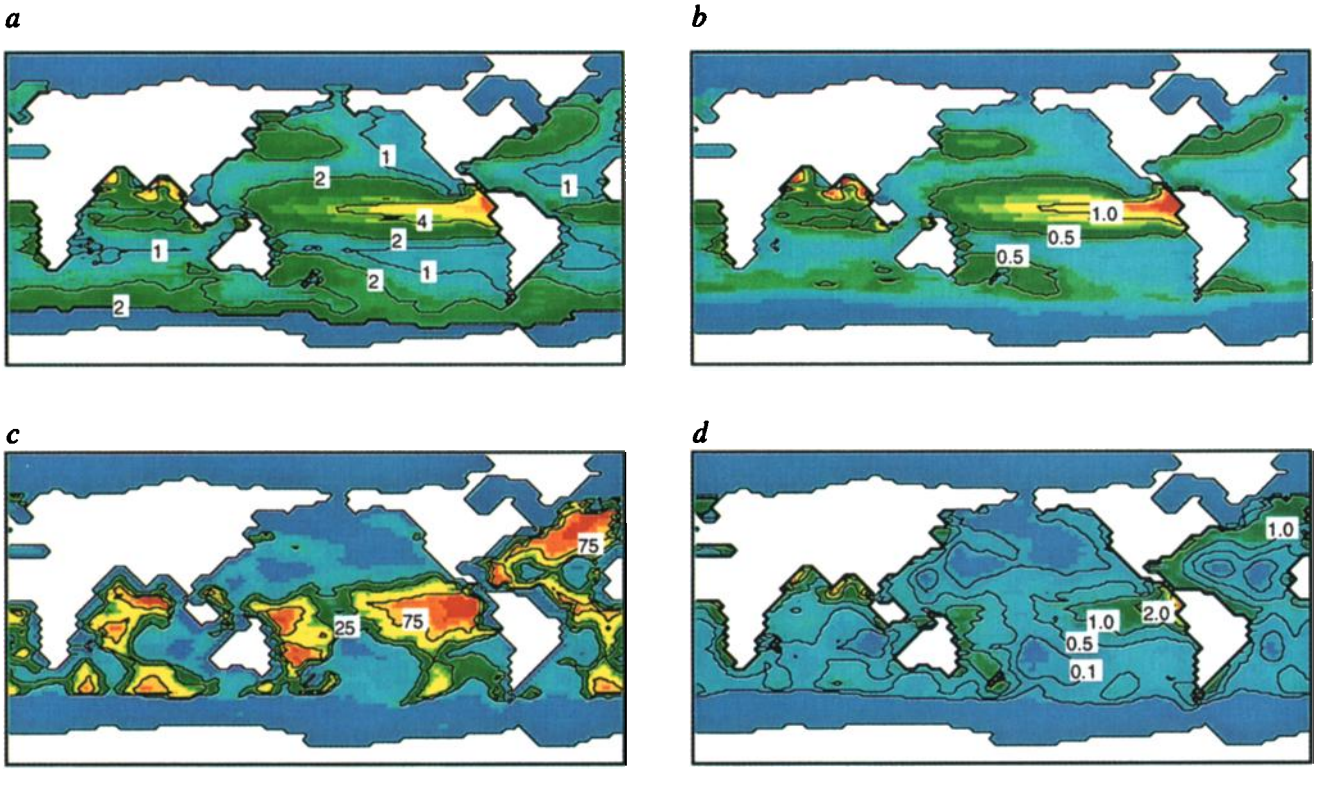


**Plate 1.** Model steady state. (a) Organic carbon export production, mol $m^{-2}$ $yr^{-1}$. (b) $CaCO_3$ export production, mol $m^{-2}$ $yr^{-1}$. (c) Sediment %$CaCO_3$, g $g^{-1}$ dry solid. (d) Sediment $CaCO_3$ mass accumulation rate, g $cm^{-2}$ $kyr^{-1}$.

approximately 20 µatm. $CaCO_3$ is produced in a 25% molar ratio to organic carbon in low and middle latitudes, resulting in the $CaCO_3$ production rate field shown in Plate 1b. Global rates of organic carbon and $CaCO_3$ export production were 7.48 and 1.65 Gt C $yr^{-1}$, respectively.

Sediment rain rates to the seafloor in the real ocean estimated from sediment trap and benthic flux studies show values of roughly 12 and 18 µmol $cm^{-2}$ $yr^{-1}$ for organic C and $CaCO_3$, respectively [*Tsunogai and Noriki*, 1991; *Archer*, 1996b; *Jahnke*, 1996], and rates close to this are required by the sediment model to reproduce the observed calcite lysocline [*Archer*, 1996b]. Coupling the ocean and the sediment models constrains the extent of water column redissolution of sinking organic carbon and $CaCO_3$, which for organic carbon was taken to be

$$\text{flux}(z) = \text{flux}(100\text{ m}) \times \left[\frac{z}{100\text{ m}}\right]^{-0.7}$$

following the form of *Martin et al.* [1987] but replacing the original coefficient 0.858 in the exponential to 0.7 to reproduce observed organic carbon fluxes to the seafloor. For water column redissolution of $CaCO_3$,

$$\text{flux}(z) = \text{flux}(100\text{ m}) \times \left[0.3 + 0.7 \times e^{-\frac{z}{2000\text{ m}}}\right]$$

where 0.3 represents the contribution of large rapidly sinking shells to the $CaCO_3$ flux. At the finite average depth of the water column, this function results in approximately 50% water column redissolution for $CaCO_3$. Particulate redissolution at depth is instantaneous, and production and decay of dissolved and suspended biogenic matter is neglected. The sediment model requires also a finite rain rate of refractory non-$CaCO_3$ material; although in the real ocean this is a regionally varying and time-varying quantity, we specify a uniform flux of 0.180 g $cm^{-2}$ $kyr^{-1}$ in pelagic sediments and values of 10 and 1 g $cm^{-2}$ $kyr^{-1}$ in grid points adjacent and once removed from land, respectively.

The sediment diagenesis model, described as the "oxygen only" model by *Archer* [1991], resolves the pore water profiles of oxygen and the carbonate buffer system to predict the dissolution of $CaCO_3$ using rain rates and overlying water chemistry as boundary conditions. The top 10 cm of the sediment are discretized into seven layers, with a minimum layer thickness near the top of 0.5 cm. The depth-integrated respiration rate within the sediment is assumed to be equal to the instantaneous sinking flux of organic carbon to the seafloor; this flux is instantly returned to the bottom ocean box. The sediment respiration rate is used to calculate the rate of $CaCO_3$ dissolution from the sediment. In the sediment, organic carbon degrades in the presence of $O_2$ with a rate constant of $2\times10^{-9}$ $s^{-1}$ and mixes into the bioturbated layer (10 cm deep) with a bulk mixing coefficient of 150 $cm^2$ $kyr^{-1}$. The solid organic carbon profile in the sediment is assumed to follow steady state balance between mixing and degradation (no time dependent mixing). $CaCO_3$ dissolution kinetics into undersaturated solution follow the rate law

$$J = k\,\frac{\text{g CaCO}_3}{\text{g solid}}\left(1 - \frac{[CO_3^{=}]}{[CO_3]_{sat}}\right)^n$$

where $k$, the dissolution rate constant, is taken to be 1 $day^{-1}$ using a rate order $n$ of 4.5 [*Archer*, 1996b], except in a comparison case where $n$=1.0 and $k$ ranges from $10^{-3}$ to $3\times10^{-5}$ $day^{-1}$. The saturation state for $CaCO_3$ is based on the concentration of carbonate ion, $[CO_3^{=}]$, relative to the saturation condition $[CO_3^{=}]_{sat}$. The heaviside function $H$ is used to prevent crystallization of $CaCO_3$ from supersaturated conditions. $CaCO_3$ is considered well-mixed within the bioturbated layer. Accumulation of $CaCO_3$ is calculated by difference between rain rate and dissolution. Maps of steady state $CaCO_3$ concentration and mass accumulation rate are given in Plates 1c and 1d.

The inventory of $CaCO_3$ on the seafloor which may become available for dissolution depends on the geometry of dissolution in surface sediments, as first described by *Broecker and Takahashi* [1978]. The zone of dissolution is isolated to the top few centimeters of the sediment surface, but bioturbation exposes sediment from below this depth, to a depth scale of about 10 cm, to the zone of dissolution. Thus at least the depth of the bioturbated layer is within reach of potential return to the ocean reservoir. If dissolution exceeds the total sedimentation rate, then the erosion of the seafloor can effectively mine old carbonates in a process called chemical erosion. Chemical erosion may continue until the entire bioturbated layer becomes filled with non-$CaCO_3$ refractory material. Thus the potential reach of dissolution, which defines the lower boundary of the "erodible inventory" of $CaCO_3$ and will be referred to as the "erodible surface", is defined as the depth to the quantity of non-$CaCO_3$ material which would be required to fill the bioturbated layer.

The inventory of $CaCO_3$ above the erodible surface is very sensitive to the porosity [*Archer*, 1996a], defined as the ratio of pore volume to total volume. The porosity of surface sediments is found empirically to vary with sediment composition. In addition, porosity is generally observed to increase in the top few centimeters of the sediment. In a fit to observations, we assume a porosity / depth relation of

$$\phi(z) = \phi_{max} + (1 - \phi_{max})\, e^{-\frac{z}{\alpha}}$$

where the depth scale $\alpha$ and the asymptotic porosity $\phi_{max}$ are chosen to be functions of the $CaCO_3$ concentration as

$$\alpha = 0.25\text{ cm} \times \frac{\%CaCO_3}{100\%} + 3.0\text{ cm} \times \left(1 - \frac{\%CaCO_3}{100\%}\right)$$

$$\phi_{max} = 1 - \frac{0.483 + 0.0045 \times \%CaCO_3}{2.5}$$

respectively. The average porosity of the bioturbated layer is then

$$\overline{\phi} = \phi_{max} - \left(\frac{\alpha(1 - \phi_{max})\left(e^{-\frac{10\text{ cm}}{\alpha}} - 1\right)}{10\text{ cm}}\right)$$

by integration. From the profiles of porosity with and without $CaCO_3$, the depth to which chemical erosion can penetrate is

$$z_{\text{erosion}} = 10\,\text{cm} \times \frac{1-\bar{\phi}_{\text{no CaCO}_3}}{1-\bar{\phi}_{\text{with CaCO}_3}} \left(1-\frac{\%\text{CaCO}_3}{100\%}\right)^{-1}$$

The global available inventory of $CaCO_3$ on the seafloor is 1770 Gt C, similar to the recent estimate of 1600 Gt C based on seafloor data [*Archer*, 1996a].

The model calculates the global rate of $CaCO_3$ dissolution and sedimentation in the ocean from the production of $CaCO_3$ in the surface ocean and from the chemistry of the bioturbated layer of the seafloor. In the model as in nature, the removal of $CO_3^=$ from the ocean by $CaCO_3$ burial is replenished by dissolution of carbonate and silicate rocks on land (terrestrial weathering). Weathering is simulated as a constant uniform input of $CO_3^=$ to surface waters at a rate of 0.145 Gt C as $CO_3^=$ per year, intended to balance the global deep sea burial rate of $CaCO_3$. This is slightly lower than estimates of riverine dissolved $CaCO_3$ fluxes [*Berner and Berner*, 1987; *Morse and MacKenzie*, 1990] plus hydrothermal exchange of Mg for Ca [*Wolery and Sleep*, 1988], although the comparison should also include shallow water deposition of $CaCO_3$, which is estimated to rival the rate of burial in the deep sea [*Milliman*, 1993]. By neglecting shallow water deposition and its corresponding weathering flux, we are implicitly assuming that these fluxes will be constant throughout the simulations. The burial rate of $CaCO_3$ is ultimately driven to balance terrestrial weathering by the mechanism of $CaCO_3$ compensation whereby ocean carbonate ion concentration ($[CO_3^=]$) increases or decreases until the fluxes balance.

The initial condition of the model is a steady state, with weathering balanced by deep sea burial, although there is some question about whether the present-day ocean has achieved this steady state following carbon cycle rearrangements accompanying the glacial termination [*Milliman*, 1993]. $CO_2$ additions from fossil fuel combustion were simulated as increases in the atmospheric concentration or in some cases by direct injection to single grid cells in the ocean model. Except for these fluxes, the coupled ocean/sediment model conserved carbon to $10^{-5}$ Gt C over 10,000 years of model integration, the expected drift due to rounding errors at the 64-bit precision of the calculation.

In addition to time dependent runs, acceleration techniques were used to obtain various steady states of the model (which will be described more fully in Section 5). A balance between weathering and the global deep sea burial of $CaCO_3$ is referred to as "global steady state" and was approached by adding $CO_3^=$ to the water column homogeneously, 10 times per century, for 800 years. The $CO_3^=$ concentration added was

$$CO_3^= \text{ added} = 50\ \mu\text{mol L}^{-1} / \text{Gt C yr}^{-1} \times [\text{ weathering - burial }]$$

The 800 year acceleration period was followed by 700 years of spin-up to allow the water column chemistry to relax toward a steady state.

A separate steady state condition can be called "local steady state," defined as a balance at each grid point between $CaCO_3$ rain, dissolution, and burial. In local steady state the $CaCO_3$ lysocline is stationary with respect to a snapshot of water column chemistry and sediment rain rates, but an ocean in local steady state can still bury less or more $CaCO_3$ than weathering and be out of global steady state. Thus the two steady state conditions are independent of each other. The local steady state condition was found by iterating seafloor $CaCO_3$ concentration at each grid point to obtain the steady state lysocline corresponding to a snapshot of water column chemistry. This operation was also followed by 1000 years of model spin-up to relax the water column chemical distribution to a steady condition. The full steady state condition, which satisfied both of these constraints, was also obtained in some cases. Note that the model neglects $CO_2$ release from metamorphic decarbonation and uptake by silicate weathering, so that full steady state of this model does not imply this balance [*Walker et al.*, 1981].

## 3. Stabilization of Atmospheric $CO_2$ Concentration

The objective of the Framework Convention on Climate Change (FCCC) is, in part, to "achieve ... stabilization of greenhouse gas concentrations at a level that would prevent dangerous anthropogenic interference with the climate system" (text available from UNEP/WMO Information Unit on Climate Change). Implementing such a stabilization will require a means of translating atmospheric concentrations into corresponding emission rates by predicting uptake by the oceans and the biota. The Intergovernmental Panel on Climate Change (IPCC) [*Schimel et al.*, 1994] has tailored a series of illustrative $CO_2$ concentration time pathways in order to study the implications of the FCCC objective. The specified $CO_2$ concentration follows arbitrary time pathways to reach various constant atmospheric concentrations ranging from 350 µatm to 1000 µatm by A.D. 2400 [*Houghton et al.*, 1996]. Various carbon cycle models have been used to estimate the rate of emissions that result in these $CO_2$ concentration time pathways [*Enting et al.*, 1994; *Wigley et al.*, 1996] by taking account of ocean and, in some cases, biospheric uptake of carbon. However, these studies have not included the effect of $CaCO_3$ dissolution. For the range of prescribed stabilization pathways, carbon emissions by A.D. 2300 have declined well below current emission rates. In this situation, low emission rates following a rise in atmospheric $CO_2$ spanning centuries, does the effect of $CaCO_3$ dissolution become apparent?

The time course of atmospheric $pCO_2$ specified by IPCC scenario s750 [*Schimel et al.*, 1994], offset by 33 µatm (Figure 1a) because the initial steady state atmospheric $pCO_2$ of the model is higher than preanthropogenic by this amount (see section 2). The allowed rate of terrestrial $CO_2$ release was determined by holding the atmospheric $CO_2$ at the specified value and tabulating the flux of $CO_2$ to the atmosphere/ocean system which was required to track this specified concentration. The results for the no-$CaCO_3$ model are given in Figure 1b; the results which included $CaCO_3$ are nearly indistinguishable on this scale. The difference between the two is plotted as absolute ocean uptake in Figure 1c and as a relative increase in Figure 1d; this is the extra $CO_2$ emission which is due to neutralization by seafloor $CaCO_3$. The extra $CO_2$ emission is at most a few percent, which is not significant relative to the uncertainty of uptake by the ocean or by the biosphere. We learn that the effect of deep sea

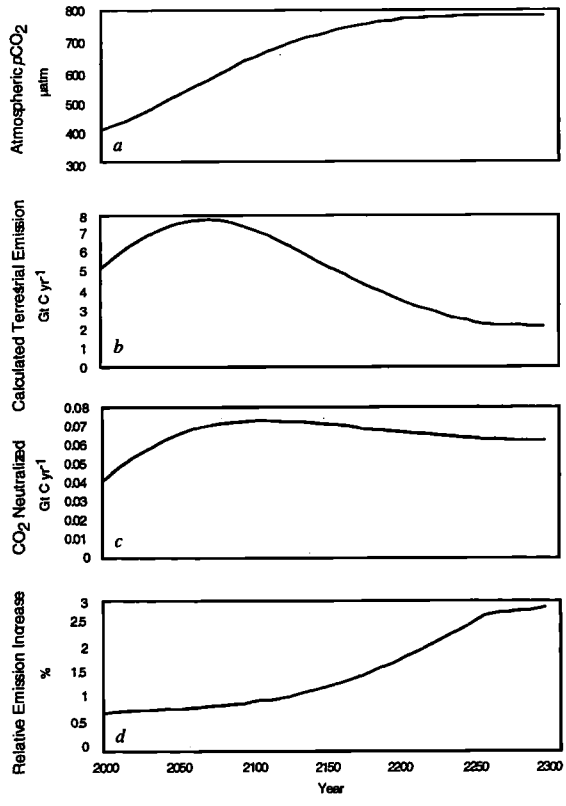


**Figure 1.** (a) Atmospheric $pCO_2$ specified by the Intergovernmental Panel on Climate Change for a case (s750) where atmospheric $CO_2$ approaches a stable concentration of 750 ppm, offset by 33 µatm because of the higher than observed model preanthropogenic $pCO_2$. (b) Calculated net terrestrial emission of $CO_2$ to match the s750 atmospheric concentration for both the $CaCO_3$ and the no-$CaCO_3$ models (which are indistinguishable from each other in the graph). The difference between the calculated emissions using the $CaCO_3$ and no-$CaCO_3$ models, in gigatons of C (c) and as a percent of net terrestrial emission (d). The kink at A. D. 2250 is the transition to a constant atmospheric $CO_2$ specified by the s750 scenario.

$CaCO_3$ dissolution on the $CO_2$ concentration over the next several centuries is likely to be negligible, consistent with previous studies [*Sundquist*, 1986; *Maier-Reimer*, 1993a; *Archer et al.*, 1997].

## 4. Deep Ocean Disposal of $CO_2$

A number of geoengineering techniques have been proposed to control atmospheric greenhouse gas concentrations or to limit potential impacts [*Panel on Policy Implications of Greenhouse Warming*, 1992]. *Marchetti* [1977] proposed capturing $CO_2$ emissions from power plants and disposing of it in the deep sea. Relative to human emissions, oceans have an immense capacity for $CO_2$, so that the added burden of $CO_2$ will be relatively small. Also, we will see in section 5 that the ultimate fate of most of the fossil fuel $CO_2$ will be to dissolve in the oceans eventually anyhow, so direct injection would only be catalyzing the transition to an already inevitable condition.

It appears that $CO_2$ retention times for the remaining atmosphere-bound fraction could exceed 500 years for marine disposal below a few kilometers [*Hoffert et al.*, 1979]. Retention times can, however, be much shorter and have been found to be dependent on the location of injection [*Haugan and Drange*, 1995]. Furthermore, there has been speculation that sediment dissolution can effectively increase the $CO_2$ residence time by preferential dissolution of $CaCO_3$ in regions near or downstream of the injection site. To assess the effect of $CaCO_3$ dissolution on ocean disposal, we have run emissions scenario A with 25% of the $CO_2$ emissions injected equally into the deep Pacific (east of Japan at 152.5° E, 31.25° N and 3000 m depth) and the Atlantic (Mediterranean outflow water at 17.5° W, 36.25° N and 3000 m depth). Figure 2 shows that the effect of injecting 25% of the fossil fuel release directly into the oceans is much more significant than is the effect of $CO_2$ neutralization by $CaCO_3$.

In addition, we have run more mechanistically interpretable "impulse injection" experiments where 10 Gt C as $CO_2$ is impulse injected into the steady state ocean, comparing Atlantic (17.5° W, 36.25° N and 3000 m depth) vs. Pacific (152.5° E, 31.25° N and 3000 m depth) both with and without $CaCO_3$. Figure 3 shows the results of these experiments. Initially, the Atlantic injection models track each other, as do the Pacific, regardless of the presence of $CaCO_3$, as we would expect. The Pacific injection is somewhat "leakier" because the Pacific is closer to the end of the line of the deep sea circulation, which leads to a faster outgassing of the atmospheric fraction of the $CO_2$ impulse and also a slight overshoot on the approach toward atmosphere/ocean equilibrium. One thousand years after the injection, the model runs sort themselves according to the presence or absence of $CaCO_3$. Dissolution fluxes (Figure 3b) are initially much higher in the Atlantic injection experiment than in the Pacific or atmospheric, and the accumulated dissolution anomaly due to the $CO_2$ injection is greatest for the Atlantic injection, presumably because of the abundance of $CaCO_3$ in Atlantic sediments. Interestingly, the atmospheric release results in greater accumulated dissolution anomaly after 1000 years than does the Pacific injection, because the pathway from the

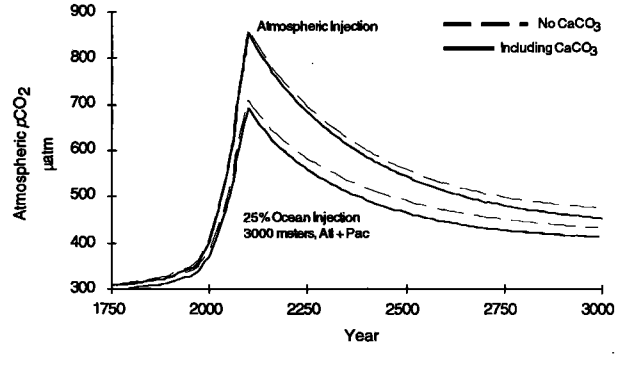


**Figure 2.** The calculated atmospheric response to a direct ocean disposal of 25% of the net terrestrial emission derrived from IPCC scenario A to the year 2100, both with and without $CaCO_3$. $CO_2$ is injected directly to two grid points, located at 3000 m depth in the Atlantic (17.5° W, 36.25° N) and Pacific (152.5° E, 31.25° N) oceans.

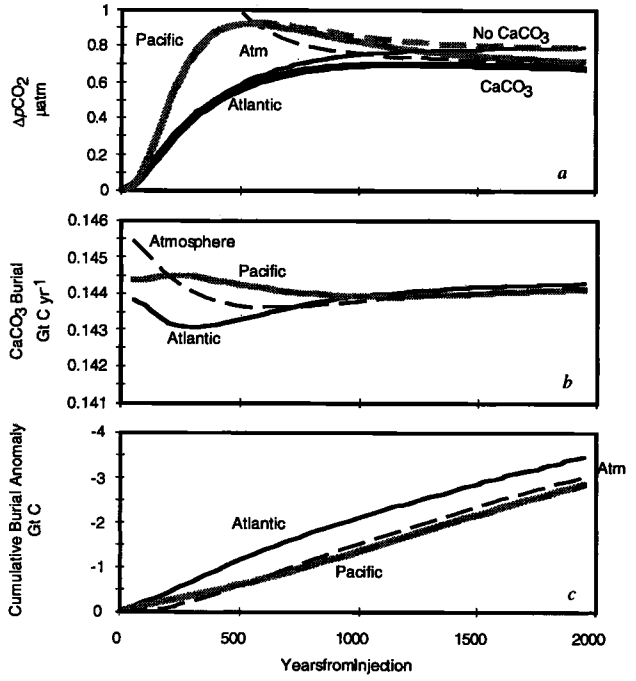


**Figure 3.** Impulse injection experiment results, comparing the effects of the location of the injection and the presence or absence of $CaCO_3$ in the model. Ten gigatons of $CO_2$ is injected into a steady state ocean (no rising atmospheric value) in the Atlantic or the Pacific oceans, both with and without $CaCO_3$, and into the atmosphere (which is equivalent to a 4.96 µatm step-increase in atmospheric $CO_2$ concentration) with $CaCO_3$ dissolution. (a) Atmospheric $pCO_2$ concentration, (b) $CaCO_3$ burial rate, and (c) cumulative burial anomaly relative to the initial steady state.

atmosphere to the ocean is through the Atlantic, which the Pacific injection skips. However, the benefits of lowering the atmospheric $CO_2$ transient by Pacific injection would appear to outweigh the drawbacks of leaking to the atmosphere and depressed $CaCO_3$ dissolution which Pacific injection appears to generate.

These results are consistent with earlier studies. *Bacastow and Dewey* [1996] speculated that $CO_2$ injection at sites near the east coast of the United States or in the North Atlantic would benefit more from calcite dissolution relative to injection in the Pacific. Using a four box model for atmosphere/ocean/sediment system, *Cole et al.* [1993, 1995] conclude that the extent of $CaCO_3$ dissolution will vary significantly with injection depth. *Nihous et al.* [1994] found extensive sediment dissolution when a model with fast dissolution kinetics was used. However, we find that the effect of enhanced $CaCO_3$ dissolution in Atlantic $CO_2$ injection (relative to atmospheric release) will only have an effect on $pCO_2$ after roughly 500 years, and this effect will likely be compensated by the enhanced production of $CO_2$ [*Kheshgi et al.*, 1994] required to carry out the capture and deep-sea injection of $CO_2$. For these reasons, we would not expect the extent of enhanced $CaCO_3$ dissolution to be an important factor in determining the effectiveness of deep sea disposal of $CO_2$.

## 5. Long Term Fate of Fossil Fuel $CO_2$

We have done a series of time dependent model integrations to characterize the millennial timescale fate of fossil fuel $CO_2$. These results have been briefly described by *Archer et al.*, [1997]; here we present a more thorough and detailed analysis. IPCC [*Houghton et al.*, 1990, 1992] has put forth families of scenarios for future emissions of $CO_2$ which have been used as benchmarks for comparing carbon cycle models [*Enting et al.*, 1994] as well as making projections of global climate change and its impacts. Using simple ocean and biosphere carbon cycle models, IPCC projected the concentration of $CO_2$ in the atmosphere in response to these emissions scenarios. Because we have no land biota model, our strategy was to impose these projected $CO_2$ concentrations on the model atmosphere beginning at an initial steady state in the year A.D. 1750. For the period from 1750 to 1990, atmospheric $CO_2$ was imposed at historical values [*Marland et al.*, 1993]. From 1990 through to A.D. 2100 we specify atmospheric concentrations at projections based on the IPCC emissions scenarios labeled "Business-as-usual" and "B" [*Houghton et al.*, 1990]. These projections include the effect of a terrestrial biospheric sink for $CO_2$. Following A.D. 2100 we chose several variants. The first two, which we label scenarios "A" and "B", follow the IPCC 1990 scenarios Business-as-usual and B, respectively, until A.D. 2100, and have zero emissions after A.D. 2100. Scenarios A22 and A23 follow Business-as-usual until A.D. 2100, then linearly extrapolate from the A.D. 2100 net terrestrial emission rate to A.D. 2200 or A.D. 2300, respectively, and thereafter the rate is set to zero. Following the emission period, no further biospheric uptake was allowed; the system was closed except for weathering and sedimentation. The rate of net terrestrial emission of $CO_2$ is shown in Figure 4, and the cumulative emissions of $CO_2$ are summarized in Table 1. Global reserves of fossil fuels have been estimated to be on the order of 5000 Gt C [*Sundquist*,

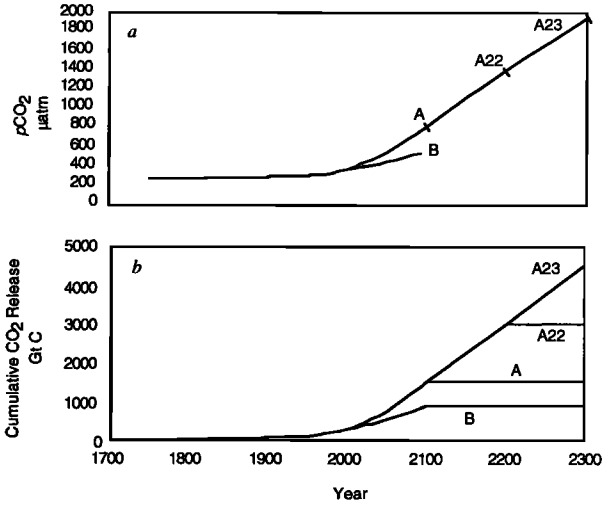


**Figure 4.** (a) Time series of atmospheric $CO_2$ concentration imposed on the model. Scenarios A, A22, and A23 stop their $CO_2$ release at the year 2100, 2200, and 2300 respectively. (b) Cumulative net terrestrial $CO_2$ release for the four scenarios.

**Table 1.** Cumulative $CO_2$ Emissions for Model Runs Driven by Extended IPCC Emission Scenerios

| Scenario | $CO_2$ Release, Gt C |
|---|---|
| B | 874 |
| A | 1506 |
| A22 | 3028 |
| A23 | 4550 |
| B Mirror | -878 |

1985], which indicates that the eventual release (beyond A.D. 2100) could greatly exceed the cumulative release of the IPCC scenarios out to A.D. 2100. The models were run both with and without $CaCO_3$ compensation until A.D. 10,000, except for A22 which was extended to A.D. 40,000.

### 5.1. $CO_2$ Invasion Timescale

Time series of atmospheric $pCO_2$ to A.D. 10,000 are shown in Figure 5. The initial increase in atmospheric $CO_2$ is determined by the emissions scenario, and the subsequent decline is caused by dissolution of $CO_2$ in the oceans (invasion) and reaction with $CaCO_3$ (neutralization). The characteristics of invasion alone can best be determined from the model results neglecting $CaCO_3$ dissolution (Figure 6a). Previous studies of the ocean uptake of a single impulse of $CO_2$ release [*Maier-Reimer and Hasselmann*, 1987; *Sarmiento et al.*, 1992] resolved $CO_2$ invasion into several distinct timescales corresponding to uptake into surface, thermocline, and intermediate and deep waters of the ocean. In our simulations, the hundred year timescale of the $CO_2$ release has obscured the shorter timescales for ocean invasion. However, we find that the overall $CO_2$ decline can be approximated with single $e$-folding timescales of 200 to 450 years, depending on

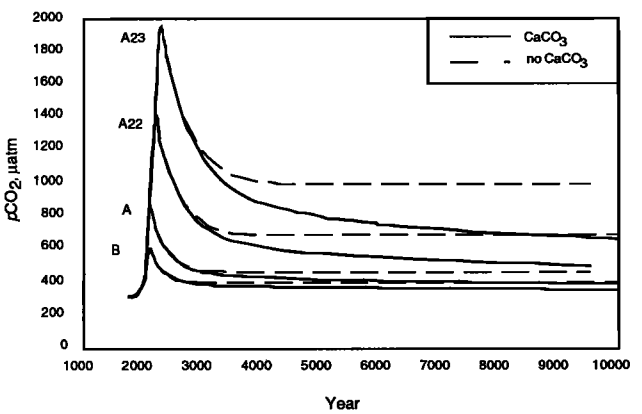


**Figure 5.** Model response to anthropogenic $CO_2$ release to the year A.D. 10,000, including the effect of $CaCO_3$ (solid curve), and neglecting $CaCO_3$ (dashed curve). The $pCO_2$ is held to IPCC projections for scenarios A and B to the year 2100 and extrapolated to the years 2200 and 2300 at the scenario A year 2100 emission rate for runs B, A, A22, and A23, respectively. After those times, a zero net terrestrial release of $CO_2$ is specified.

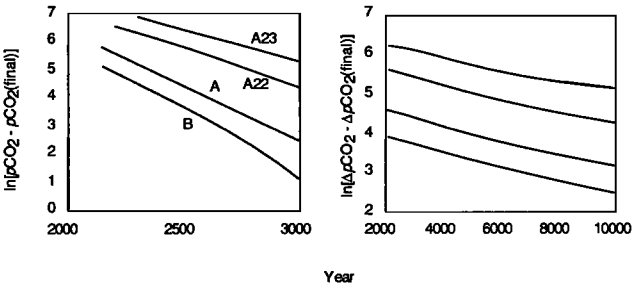


**Figure 6.** (a) The $e$-folding time for invasion of $CO_2$ into the oceans can be estimated from the slope of the log of the model $pCO_2$ (in microatmospheres) for the case of no $CaCO_3$ dissolution (model - initial) versus time. The timescale is 250-400 years, longer for higher $CO_2$ release scenarios. (b) The timescale for the effect of $CaCO_3$ on the $pCO_2$ of the atmosphere can be estimated from the slope of the log of the difference between the model runs with and without $CaCO_3$ versus time, $\Delta pCO_2$, defined as

$$\Delta pCO_2 = \left(pCO_{2_{\text{with CaCO}_3}} - pCO_{2_{\text{CaCO}_3,\text{final}}}\right) - \left(pCO_{2_{\text{no CaCO}_3}} - pCO_{2_{\text{no CaCO}_3,\text{final}}}\right)$$

This timescale appears to be about 5000 years and relatively independent of the $CO_2$ release magnitude.

the amount of $CO_2$ released (Table 2). When $CaCO_3$ dissolution is disallowed in the model, the final equilibrium between the ocean and the atmosphere finds 70%-81% of the fossil fuel release sequestered in the oceans (Table 2). These results are consistent with *Sundquist* [1990b].

### 5.2. Reaction with $CaCO_3$

The long-term effects of $CaCO_3$ weathering and seafloor dissolution on the $pCO_2$ of the atmosphere can be seen as the divergence between the solid curves (including $CaCO_3$) and the dashed lines (no $CaCO_3$) in Figure 5. In the initial millennium, there is little difference between the two model formulations, but beyond A.D. 3000, the reaction of $CO_2$ with $CaCO_3$ becomes significant. The pH equilibrium chemistry of dissolved $CO_2$ leads to an inverse relationship between $CO_2$ and $CO_3^=$, which can be seen as a decrease in deep Pacific $[CO_3^=]$ following the $CO_2$ invasion (Figure 7). This, in turn, provokes two distinct but complementary neutralization responses: dissolution of previously deposited $CaCO_3$ on the seafloor and net dissolution of terrestrial $CaCO_3$ which is temporarily not balanced by seafloor deposition of $CaCO_3$. This distinction will be justified in section 5.5.

By the end of the simulations, significant fractions of the global inventories of $CaCO_3$ in the bioturbated layer and within reach of chemical erosion have been exhausted. The initial $e$-folding time for the removal of $CO_2$ by $CaCO_3$, relative to the case of no $CaCO_3$, is 5-6 kyr and relatively independent of the magnitude of $CO_2$ release (Figure 6b and Table 2), based on a plot of the log of the increase in the $\Delta pCO_2$ ($CaCO_3$ - no $CaCO_3$) toward the final steady state value given in Table 2. As we shall see, this can be taken to be the timescale of "seafloor" neutralization effect on the $pCO_2$ of the atmosphere.

**Table 2.** Summary of Ocean Effects in the Model Analyses of the Extended IPCC Emission Scenarios

| | B | A | A22 | A23 |
|---|---|---|---|---|
| Initial alkalinity Gt C equivalents[a] | 40510 | 40510 | 40510 | 40510 |
| Initial $CO_2$ inventory Gt C | 38400 | 38400 | 38400 | 38400 |
| Initial erodible $CaCO_3$ Gt C[b] | 1570 | 1570 | 1570 | 1570 |
| Initial $pCO_2$ | 310 | 310 | 310 | 310 |
| Invasion $\tau$, yr[c] | 212 | 255 | 365 | 453 |
| Invasion final $pCO_2$[d] | 394 | 463 | 685 | 995 |
| Invasion $CO_2$ uptake[e], % | 80.7 | 79.6 | 75.1 | 69.7 |
| Seafloor neut. $\tau$, yr (<A.D. 10,000)[f] | 5480 | 5490 | 5870 | 6810 |
| Seafloor neut. $pCO_2$ | 355 | 390 | 497 | 661 |
| Seafloor neut. $CO_2$ uptake[g], % | 9.0 | 9.8 | 12.5 | 14.8 |
| Seafloor neut. final alkalinity[a] | 41611 | 42337 | 43831 | 44761 |
| Seafloor neut. erodible $CaCO_3$[b] | 1230 | 975 | 424 | 129 |
| Terr. weat. $\tau$[y] | | | 8260 | |
| Equilibrium[h] $pCO_2$ | 343 | 366 | 425 | 489 |
| Equil.[h] $CO_2$ uptake, % | 2.9 | 3.2 | 4.8 | 7.6 |
| Equil.[h] alkalinity[l] | 42015 | 43060 | 45588 | 48104 |
| Equil.[h] $CO_2$ atm. residual[e], % | 7.5 | 7.4 | 7.6 | 7.9 |

[a]The ocean inventory of alkalinity, scaled to be directly comparable to carbon inventories. The scaling factor is 12 g $eq^{-1}$.

[b]Expressed in mass of C, not $CaCO_3$, for direct comparison with other carbon inventories.

[c]Determined by linear regression of $\ln[pCO_2(t) - pCO_2(\text{final})]$ versus time for a time interval $2250 < t < 3000$ A.D.

[d]Final $pCO_2$ of the model neglecting $CaCO_3$.

[e]Expressed as percentage of the released $CO_2$

[f]Determined by linear regression of the log of approach to the full effect of $CaCO_3$ on $pCO_2$, versus time as defined in the caption to Figure 6b. Regression was performed on model results $2000 < t < 10000$. Final $pCO_2$ values for the $CaCO_3$ experiments are taken from the equilibrium results (see footnote h).

[g]Same as footnote f but over time interval $10,000 < t < 40,000$. Model results for the A22 scenario only.

[h]Determined by acceleration of the model to steady state where weathering is balanced by burial and the lysocline is in local equilibrium with the water column saturation horizon.

None of the model results in Figure 5 have reestablished equilibrium by the end of their 10 kyr runs. This can be seen in Figure 7c as the imbalance between weathering and deep sea $CaCO_3$ accumulation and the depletion of the seafloor $CaCO_3$ inventory relative to the initial (steady state) condition. Figure 8 shows A22 to the year 40,000, by which time the global ocean burial rate and the seafloor $CaCO_3$ inventories appear to have largely returned to their original values. The *e*-folding timescales for the approach to weathering / accumulation steady state ("terrestrial neutralization") can be estimated from semilog plots in Figure 9. In the first 10 kyr, both the atmospheric $CO_2$ decline and the recovery of weathering / burial steady state relax to their final states with *e*-folding timescales of 5.5-6.8 kyr (Figure 9a). After the year 10,000, the slope shallows to an 8.3 kyr timescale. This is because the seafloor $CaCO_3$ inventory has reached a minimum value and has been exhausted as a source of alkalinity to neutralize $CO_2$ (see section 5.5). The remaining source, terrestrial $CaCO_3$, is slower than seafloor neutralization. The replenishment of the seafloor $CaCO_3$ inventory after the year 20,000 appears to take place with an *e*-folding timescale of 18 kyr (Figure 9c).

The division of $CaCO_3$ compensation response of the ocean into several components has been a common finding of previous studies. *Sundquist* [1990a] partitioned the alkalinity response of the ocean into primary and secondary responses based on the log slope of the model response; these responses

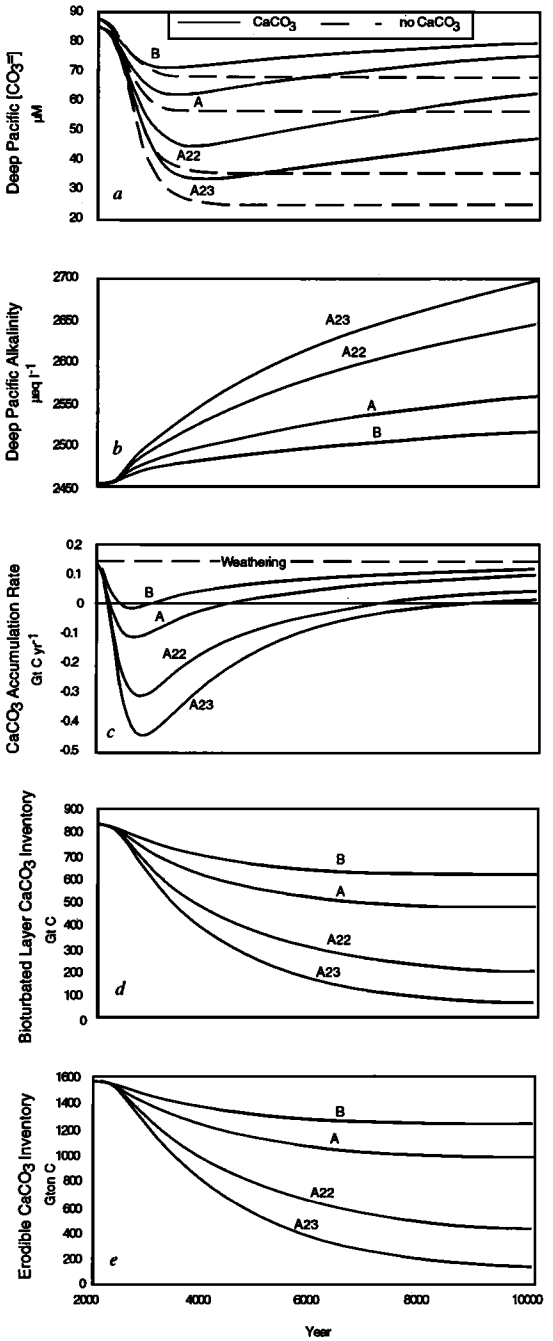


**Figure 7.** Model response to the year A.D. 10,000 of (a) deep Pacific $[CO_3^=]$. (b) Alkalinity of the deep Pacific ocean. (c) Global accumulation rate of $CaCO_3$ with negative values denoting net erosion. (d) Inventory of $CaCO_3$ within the bioturbated layer on the seafloor. (e) Inventory of $CaCO_3$ within the potential reach of chemical erosion on the seafloor.

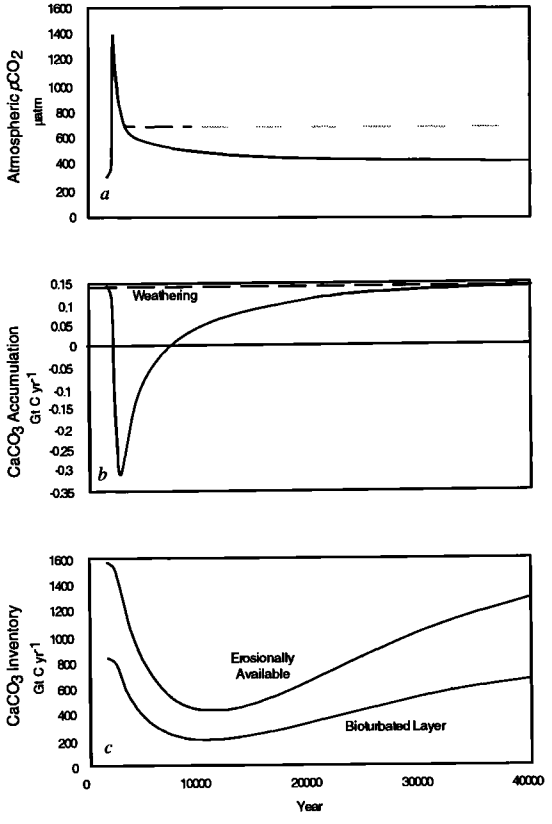


**Figure 8.** Model results of (a) atmospheric $pCO_2$, (b) $CaCO_3$ accumulation rates, and (c) $CaCO_3$ inventories for the A22 emission scenario integrated to the year A.D. 40000.

ranged from 1500 to 2700 and 10,800 to 14,200 years, respectively. The former was identified as seafloor neutralization, because it was sensitive to sediment dissolution kinetics, while the latter corresponds to the $CaCO_3$ compensation (weathering / burial imbalance) timescales as estimated by *Broecker and Peng* [1987] and *Boyle* [1983]. *Walker and Kasting* [1992] assumed as an upper limit that seafloor dissolution occurs instantaneously, so that the several thousand year response time of their model to fossil fuel invasion represents only what we have called terrestrial neutralization.

### 5.3. $CaCO_3$ Steady State

The final state of the 40 kyr A22 integration has nearly restored the seafloor $CaCO_3$ inventory to original values, and the global burial rate balances weathering. This state has also been obtained directly by the acceleration technique described in section 2. The resulting alkalinity of the ocean and $pCO_2$ of the atmosphere are given in Table 2. We find that even after complete reaction with $CaCO_3$, approximately 7-8% of the fossil fuel $CO_2$ remains in the atmosphere, consistent with *Sundquist* [1990a] and *Walker and Kasting* [1992]. The equilibrium partitioning of fossil fuel $CO_2$ between the atmosphere and the $CaCO_3$-buffered ocean can be understood from the aqueous $CO_2$ equilibrium reactions. Dissolved $CO_2$ equilibrium can be expressed as

$$\frac{pCO_2\left[CO_3^{=}\right]}{\left[HCO_3^{-}\right]^2} = \frac{K_2' K_H}{K_1'} = \text{constant}$$

which relates the partial pressure of $CO_2$ exerted by a seawater sample and the concentrations of carbonate and bicarbonate ions to the apparent dissociation constants for carbonic acid ($K_1'$ and $K_2'$) and the Henry's law solubility product for $CO_2$ ($K_H$). For the global ocean and atmosphere, the situation is complicated by heterogeneities in ocean chemistry and temperature, but we will retain the idea that the ratio on the left hand side will behave as a nearly constant value as the carbon inventories of the ocean and atmosphere change. Taking the ratio of initial and final states of the ocean/atmosphere and rearranging, we get the approximation

$$\frac{pCO_{2_{final}}}{pCO_{2_{initial}}} \approx \left(\frac{HCO_{3_{final}}^{-}}{HCO_{3_{initial}}^{-}}\right)^2 \frac{CO_{3_{initial}}^{=}}{CO_{3_{final}}^{=}}$$

where the constants have canceled and where we now replace

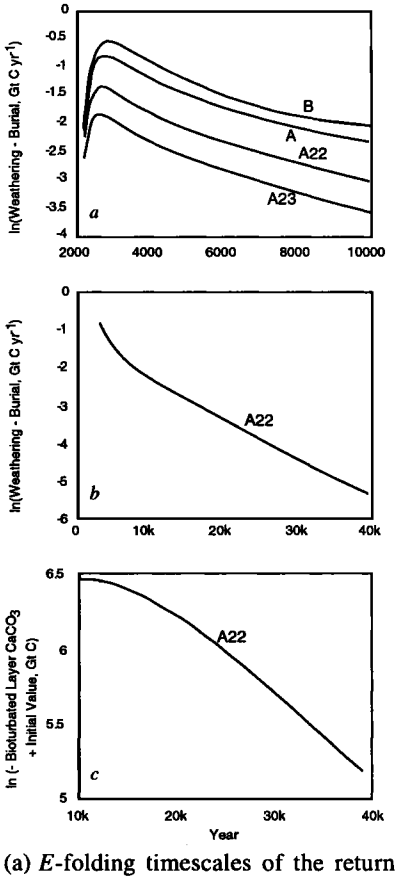


**Figure 9.** (a) *E*-folding timescales of the return to a balance between weathering and burial of $CaCO_3$ for the A22 scenario. Slope of curves from A.D. 2000 to A.D. 10000 indicates timescales of 5480-6810 years (see Table 2). (b) Return to weathering / burial steady state over 40 kyr of model time, A22 scenario. The relaxation timescale slows to 8260 years after the year A.D. 10,000. (c) The timescale for restoration of the equilibrium depth of the lysocline is 18.1 kyr from the 40 kyr A22 model results, based on the log of the bioturbated layer $CaCO_3$ inventory relative to the initial value.

concentrations of bicarbonate and carbonate with global inventories, which we denote by dropping the brackets. Equilibrium with $CaCO_3$ (the neutralization reaction) tends to restore $CO_3^=$ to close to its initial (equilibrium) value, reducing the final factor on the right hand side to near 1. This leaves atmospheric $pCO_2$ to scale with the bicarbonate inventory of the ocean squared. We make a final approximation that the relative increase in ocean bicarbonate should be about the same as the relative increase in total carbon in the ocean, since bicarbonate is the dominant form of carbon while the second most important form, carbonate ion, is held constant. This leaves us with the approximate relation

$$\frac{pCO_{2_{final}}}{pCO_{2_{initial}}} \approx \frac{\left(\Sigma CO_{2_{ocean}} + 2 \times CO_{2_{ff}}\right)^2}{\Sigma CO^2_{2_{ocean}}}$$

where the final total $CO_2$ inventory of the ocean is approximated as the initial value plus twice the fossil fuel $CO_2$ release; the factor of 2 is due to the nearly 1:1 reaction of $CO_2$ with $CaCO_3$, which releases additional carbon to the ocean. For the A22 scenario, the initial total $CO_2$ inventory is 38,400 Gt C, the fossil fuel release is 3028 Gt C, and the predicted equilibrium $pCO_2$ is 34% higher than the initial value (compared with 37% observed in the full model), accounting for 6.7% of the fossil fuel release (compared with 7.6% observed in the full model). We conclude that the residual $CO_2$ left in the atmosphere after complete reaction with $CaCO_3$ is a straightforward result of equilibrium chemistry of inorganic carbon. This result is therefore likely to be relatively robust and model independent.

The atmospheric residual will be buffered by the silicate rock cycle, which would tend toward equilibrium between $CO_2$ consumption associated with weathering of basic components of silicate rocks such as CaO, and the reverse of this reaction, metamorphic decarbonation and volcanic degassing of $CO_2$ [*Walker et al.*, 1981; *Berner et al.*, 1983]. This mechanism is thought to stabilize atmospheric $CO_2$ on a time frame of several hundred thousand years. The long time frame for this mechanism, relative to the glacial / interglacial cycles, raises the question of what value for atmospheric $CO_2$ is required to achieve balance between weathering and metamorphism. The question is complicated by fluctuations in both atmospheric $CO_2$ and presumably in silicate weathering associated with the climate cycles, but presumably the true equilibrium $CO_2$ value is somewhere between the glacial and interglacial values.

The 7-8% atmospheric residual of the fossil fuel $CO_2$ would, according to our current understanding, raise the baseline atmospheric $CO_2$ concentration for a period of several hundred thousand years. This long tail on the fossil fuel $CO_2$ forcing of climate may well be more significant to the future glacial/interglacial timescale evolution of Earth's climate than will the brief period of greater intensity warming, since its duration is greater than a glacial cycle. The end result of a 3000 Gt fossil fuel release (scenario A22) will be an atmospheric $pCO_2$ value of approximately 400 ppm. This represents an increase in the direct radiative forcing from $CO_2$, relative to the preanthropogenic concentration of 280 ppm, that is as large as the $CO_2$ direct radiative forcing change on the glacial termination (from 200 ppm).

### 5.4. Sensitivity to $CaCO_3$ Dissolution Kinetics

Dissolution of $CaCO_3$ in the laboratory has been shown to exhibit a nonlinear dependence on the undersaturation of the solution, attributed to dissolution as the sum of a range of elementary reactions ($CaCO_3$ reacting by itself to produce $Ca^{2+}$ + $CO_3^=$ or reactions coupled with $H^+$ or $H_2CO_3$) and a range of types of crystal sites (corner and defect sites as opposed to flat surface sites) [*Berner and Morse*, 1974]. A dissolution order $n$ of 4.5 has been observed in the laboratory by *Keir* [1980], and has been assumed by in situ dissolution rate studies [*Archer et al.*, 1989; *Berelson et al.*, 1990; *Cai*, 1992], although the dissolution order is difficult to constrain using the range of saturation conditions found in the deep sea [*Hales et al.*, 1993]. Recently, *Hales* [1995] has argued that first-order rate kinetics ($n$=1) may be more appropriate for in situ conditions. Hales finds that the range of rate constant values $k$ inferred from his in situ data spans nearly 3 orders of magnitude, while the same data can be fit using $n$=1 with only 1 order of magnitude variation, using $k$ values between 0.1 and 0.01% $day^{-1}$.

The effect of higher order dissolution kinetics is to increase the sensitivity of the dissolution rate to the degree of undersaturation as undersaturation becomes more extreme. Within the diffusive pore water medium, the effects of the dissolution rate constant are more difficult to predict, because the differences in the microscopic rate law may be compensated for by changes in the diffusion/reaction steady state pore water concentration profiles. In any case, we expect that the differences between the two formulations may become pronounced during the extreme acidification of the ocean after fossil fuel uptake. For the deep sea, undersaturation values

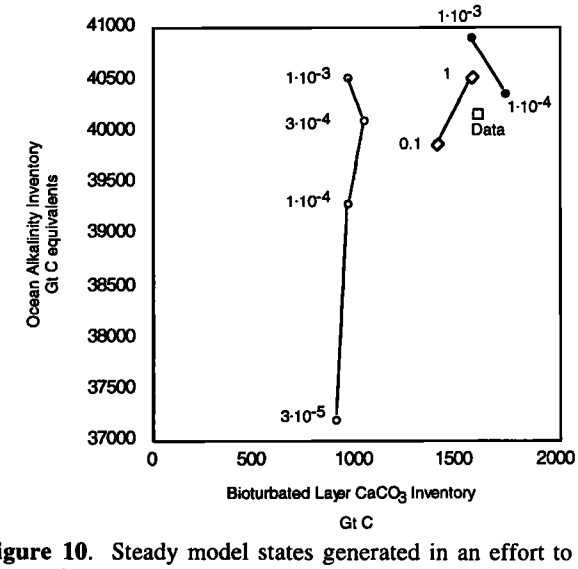


**Figure 10.** Steady model states generated in an effort to tune the model for linear dissolution kinetics. Equilibrium model dependence of alkalinity and $CaCO_3$ inventories on weathering rate (equal to 0.145 Gt C $yr^{-1}$ for open symbols and 0.175 Gt C $yr^{-1}$ for solid circles). Circles are the linear rate law model with rate coefficients ranging from $3 \cdot 10^{-5}$ to $1 \cdot 10^{-3}$ $d^{-1}$ as indicated. Diamonds are 4.5 order rate law (nonlinear) model with rate coefficients of 1 and 0.1 $d^{-1}$ as indicated. The square is a data-based estimate from the real ocean.

(expressed as $\Delta CO_3 = [CO_3^=] - [CO_3^=]_{saturation}$) as low as -40 μmol $kg^{-1}$ are observed in the deep Pacific, but calcite is generally completely depleted from these sediments; the range of $\Delta CO_3$ across the lysocline is of order 20-30 μmol $kg^{-1}$ in $\Delta CO_3$. Across this range in undersaturation, the difference between 1.0 and 4.5 order kinetic rate laws may be rather subtle. In contrast, deep sea $[CO_3^=]$ suddenly decreases 60 μmol $kg^{-1}$ following a large fossil fuel $CO_2$ release (Figure 7), in contact with sediments where $CaCO_3$ has not yet been depleted. Under these conditions, the two kinetic rate laws may differ significantly in their neutralization and $CaCO_3$ compensation responses.

The comparison between linear and nonlinear $CaCO_3$ dissolution kinetics required first spinning up the model to a steady state using linear dissolution kinetics in the sediments. We found that simply changing the dissolution order and rate constant to linear kinetics consistently underrepresented the inventory of $CaCO_3$ in surface sediments (Figure 10). This becomes significant as $CaCO_3$ is depleted from surface sediments; the lower inventory decreases the dissolution flux, obscuring the differences between the two kinetics formulations. Linear kinetics generate a lower $CaCO_3$ inventory when everything else is equal because the lysocline tends to be sharper using linear kinetics. For a given weathering rate (which determines the area of high-$CaCO_3$ sediments where most of the $CaCO_3$ burial occurs), there is a smaller area of moderate-$CaCO_3$ concentration sediments to contribute to the $CaCO_3$ inventory using linear kinetics; $CaCO_3$ concentration tends to be more focused into areas of high accumulation. Varying the dissolution rate constant $k$ had the effect in the steady state of changing the saturation state of the whole ocean (represented in Figure 10 by the alkalinity inventory), without much of a change in the bioturbated layer $CaCO_3$ inventory, which is determined by the global burial rate. In other words, the rate constant affects the $\Delta CO_3$ of the lysocline without changing the thickness of the transition zone very much. We found that to reproduce both the alkalinity and the $CaCO_3$ inventories of the nonlinear model, we were forced to increase the weathering rate from 0.145 Gt C $yr^{-1}$ to 0.175 Gt C $yr^{-1}$, thus increasing the global burial rate of $CaCO_3$. However, the global burial rate is not known to this precision, so that the contrast in burial rates cannot be construed as an argument either for or against linear kinetics.

A comparison of the global burial rate of $CaCO_3$ is presented as deviations from the initial steady state value in Figure 11. We see that for $n$=1 and $k$=$10^{-3}$ $day^{-1}$ (the fast linear model) the results are indistinguishable from the results using $n$=4.5 and $k$=1 $day^{-1}$ (the nonlinear model). This is also true for the slow nonlinear model ($n$=4.5 and $k$=0.1 $day^{-1}$). However, when $n$=1 and $k$=$10^{-4}$ $day^{-1}$ (the slow linear model) the initial spike in dissolution intensity is attenuated, but the long-term trend in dissolution converges on the time trend of the other models. The $CO_2$ histories of the three models are shown in Figure 11b, and again we find relatively minor differences. The slow nonlinear model lags in the uptake of fossil fuel $CO_2$ by about 10 ppm throughout the simulation, while the $pCO_2$ of the fast linear model is consistently about 5 ppm lower than the nonlinear model (largely an offset due to the difference in steady state initial conditions). The

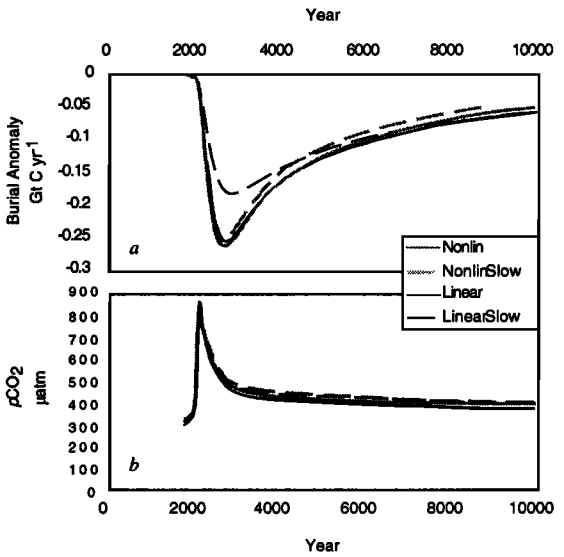


**Figure 11.** (a) $CaCO_3$ burial anomaly (deviation from steady state value) and (b) atmospheric $pCO_2$, a comparison between linear (first order) versus nonlinear (4.5 order), and fast versus slow dissolution kinetics. Rate constants are as follows: nonlinear, 1.0 $day^{-1}$; nonlinear slow, 0.1 $day^{-1}$; linear, $1{\cdot}10^{-3}$ $d^{-1}$; linear slow, $1{\cdot}10^{-4}$ $day^{-1}$. Weathering rates are 0.145 Gt C $yr^{-1}$ for nonlinear models and 0.175 Gt C $yr^{-1}$ for linear models.

formulation of the kinetic rate law has surprisingly little effect on the neutralization of fossil fuel $CO_2$, except for the magnitude of the dissolution spike immediately following invasion for the slow linear model, and interestingly, only the linear model is sensitive even in this time period. The dynamics of the dissolution spike are explored below.

### 5.5. Analysis and Discussion

**5.5.1. A Phase Diagram for $CaCO_3$ Compensation.** Anthropogenic $CO_2$ can be viewed as a perturbation of two natural cycles of carbon on the surface of the earth: $CaCO_3$ compensation in the ocean and the silicate rock weathering / volcanic degassing balance [*Walker et al.*, 1981; *Berner et al.*, 1983]. The interaction of the $CO_2$ perturbation with these natural cycles is controlled by the dynamics of the system, which we undertake to analyze here. These dynamics will also eventually apply to our understanding of carbon cycle rearrangements corresponding to the glacial interglacial transitions.

The response of the model to fossil fuel invasion is a relaxation toward a new steady state condition. An analogy can be drawn to the dissolution of a solid material in a beaker in the lab. The kinetics of this system are described by rate equations, which will require at least two pieces of information, the extent of disequilibrium (in this case a property of the solution) and the quantity of the solid phase reactant (or more precisely the surface area). We will characterize the dynamics of the ocean/sediment model by ignoring spatial heterogeneity and reducing the complex three-dimensional calcite saturation state (defined by the deviation of $CO_3^=$ from saturation, $\Delta CO_3$) and $\%CaCO_3$ fields

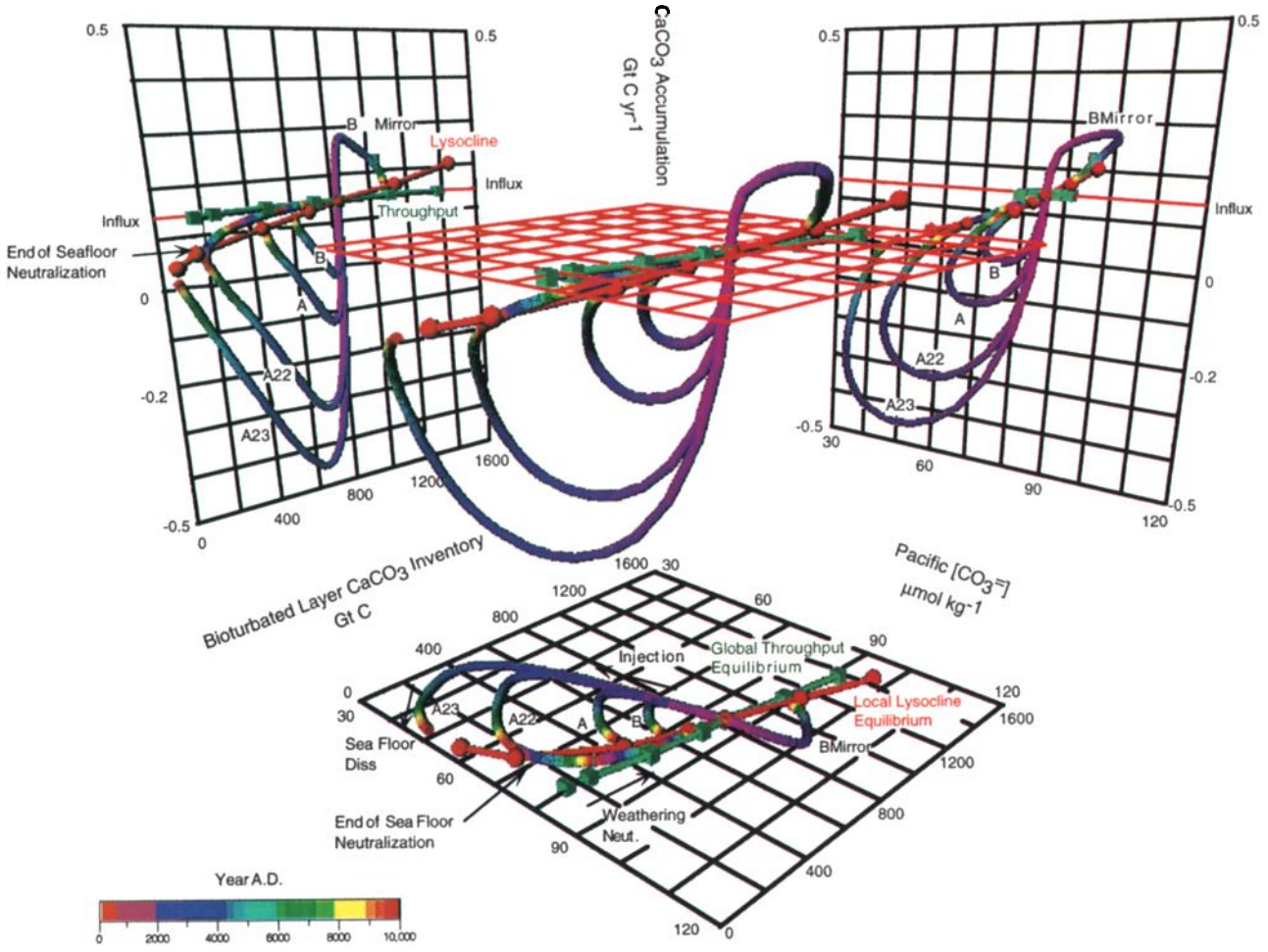


**Plate 2.** The two variables which largely determine the global accumulation rate of $CaCO_3$, deep ocean $[CO_3^=]$ and the bioturbated layer $CaCO_3$ inventory, are plotted against the model $CaCO_3$ burial rate response. Spheres and the red line represent synchrony between the calcite lysocline and the water column saturation state (the steady lysocline regime). Cubes and the green line represent the state of weathering / burial steady state for $CaCO_3$ (the steady throughput regime). Time dependent response to $CO_2$ invasion is shown as multicolored lines, with model time indicated by the color scale, which resets to zero every 10 kyr for the 40 kyr A22 scenario run. Initial invasion of $CO_2$ depletes deep ocean $[CO_3^=]$, which is subsequently replenished as mixed layer $CaCO_3$ is depleted. Once the model trajectory intersects the steady lysocline line, neutralization of $CO_2$ by chemical erosion ceases. Symmetry of the model response is shown by removing $CO_2$ from the atmosphere in a mirror image to scenario B, which traces a complementary path to B.

to single values. These values will be the concentration of $CO_3^=$ from a single arbitrary location in the western equatorial Pacific (170°W, 1.25°S and 2000 m) representing the saturation state, and the global inventory of $CaCO_3$ in the sediment bioturbated layer, representing the surface area of substrate. By reducing the state of the ocean to these two variables, we are assuming that the ocean state associated with a given value of one of these variables is single valued, in other words that a single pair of numbers is all that is required to describe the carbon cycle in the ocean. Of course, the state of the ocean cannot be exactly represented by these two variables alone. However as we will show, this approximation simplifies our interpretation of the behavior of the model as a dynamical system. Also, we shall see that the limitations of this approach are themselves revealing of the dynamics of the model

These two state variables for the ocean carbonate system correspond to reservoirs for carbonate with fluxes between them. The reservoirs are the $[CO_3^=]$ of the ocean, determined by the alkalinity and $\Sigma CO_2$, and the inventory of seafloor $CaCO_3$ available for dissolution (Figure 12). The input to the system is weathering, which transfers alkalinity to the ocean Output consists of the imbalance between the rain rate of $CaCO_3$ to the seafloor and the seafloor dissolution flux, which we will call the "accumulation" rate of $CaCO_3$ (the middle arrow in Figure 12). Finally, $CaCO_3$ is effectively removed from the system as it escapes the potential reach of seafloor dissolution. The final removal of sediment from the ocean system will be called "burial," the bottom arrow in Figure 12 Because the burial rate is defined relative to the deepest possible reach of chemical erosion, its value can never be negative, since by definition $CaCO_3$ below the erodible depth

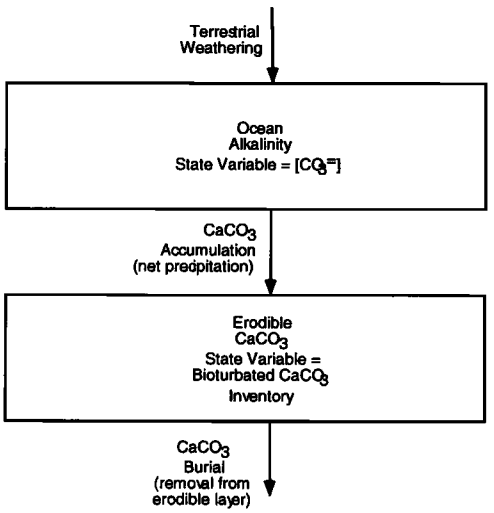


**Figure 12.** Fossil fuel neutralization can be conceptualized as a perturbation to the system of weathering, $CaCO_3$ accumulation (defined as the instantaneous difference between $CaCO_3$ deposition and dissolution), and burial (defined as the permanent removal of $CaCO_3$ from the potential reach of chemical erosion, or the flux of $CaCO_3$ past the erodible line in the sediments, defined in text).

can never be redissolved. The rate of burial as defined here is determined by the accumulation rate of non-$CaCO_3$ material on the seafloor multiplied by the concentration of $CaCO_3$ at the erodible depth.

**5.5.2. Stages of the Neutralization Process.** The differential equation describing ocean $[CO_3^=]$ is

$$\frac{\partial[CO_3^=]}{\partial t} = \alpha \times [\text{weathering} - \text{accumulation}] - \beta \times CO_2 \text{ invasion} \quad (1)$$

where $\alpha$ and $\beta$ represent buffering of ocean $[CO_3^=]$ by the reaction with dissolved $CO_2$. These coefficients are nonlinear functions of the concentrations of $CO_3^=$, $HCO_3^-$, and $CO_2$ but are always positive, so that an excess of weathering over accumulation always drives an increase in ocean $[CO_3^=]$, $CO_2$ invasion always decreases ocean $[CO_3^=]$, and a balance between weathering and accumulation, in the absence of $CO_2$ invasion, is the steady state. Beyond this, the complexity intrinsic to $\alpha$ and $\beta$ need not concern us here.

The equation for the bioturbated layer $CaCO_3$ inventory is

$$\frac{\partial \text{erodible } CaCO_3}{\partial t} = \text{accumulation} - \text{burial} \quad (2)$$

where accumulation is defined as the net sedimentation rate, which can be negative indicating chemical erosion, and burial is the rate at which $CaCO_3$ crosses the erodible depth and becomes unavailable for chemical erosion, a flux which by definition can never be negative. We leave a detailed characterization of these fluxes, in particular the accumulation flux, to section 5.5.3 but for the time being it is instructive to derive numerically the steady state conditions for these two variables, where the input and output fluxes balance and the time derivatives equal zero.

The steady state condition for the erodible $CaCO_3$ inventory (equation 2) is the condition of local balance in the budget for $CaCO_3$ in the sediment mixed layer, where at each model grid point

$$CaCO_3 \text{ rain} = \text{dissolution} + \text{burial}$$

For any distribution of $[CO_3^=]$, there is a concentration field of $CaCO_3$ on the seafloor which satisfies this condition. Because the equilibrium condition can be calculated locally, this steady state condition will hereafter be called local lysocline equilibrium. The set of local lysocline equilibrium states can be described by a line on a deep Pacific $[CO_3^=]$ / bioturbated layer $CaCO_3$ phase plot (Figure 13a). This line was calculated by (1) adjusting the $[CO_3^=]$ of the deep sea by imposing a homogeneous offset to the total $CO_2$ of the water column, then (2) calculating the steady state concentration of $CaCO_3$ by

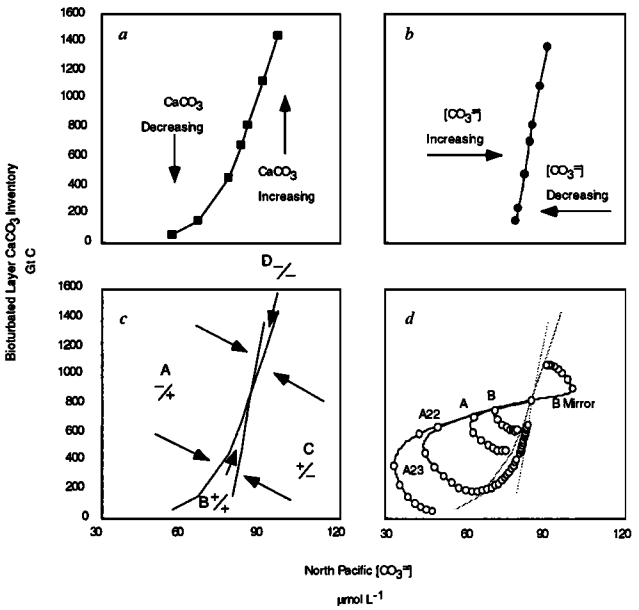


**Figure 13.** (a) Steady state concentration of $CaCO_3$ at each grid point on the seafloor as a function of $[CO_3^=]$ at an arbitrary location in the Pacific Ocean (170°W, 1.25°S and 2000 m). Above this "steady lysocline" line, the $CaCO_3$ decreases with time, and below this it increases. Vertical axis is the global inventory of $CaCO_3$ in the bioturbated layer. (b) Deep Pacific $[CO_3^=]$ at which the ocean $CaCO_3$ accumulation rate balances the terrestrial weathering rate, as a function of the $CaCO_3$ inventory results of Figure 13a. To the left of the "steady throughput" line ocean $[CO_3^=]$ increases, to the right it decreases. (c) Time dependent behavior of both variables, $[CO_3^=]$ and $CaCO_3$, from Figures 13a and 13b tends to drive the model state toward one of the regions B or D. The full model steady state is given by the intersection of the steady lysocline and the steady throughput lines. (d) Model behavior for the IPCC B, A, A22, and A23 scenarios (see Table 1). Circles mark millennia. Simulations started in steady state, and all went to 10 kyr except for the A22 scenario, which went to 40 kyr, long enough to return to show the behavior of the return toward steady state. The "B Mirror" scenario is merely the opposite of the "B" scenario, with a $CO_2$ drawdown flux that mirrors the $CO_2$ release flux of the B scenario.

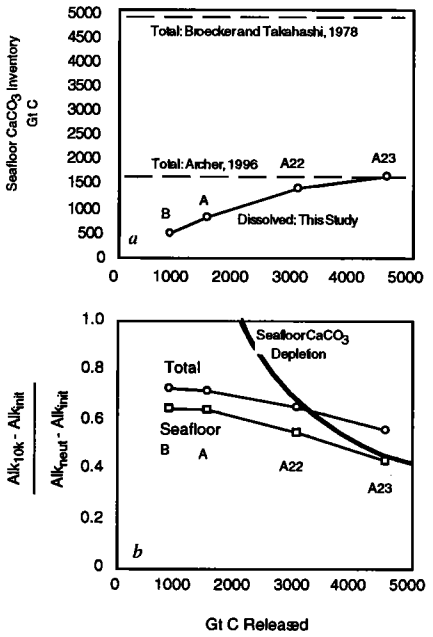


**Figure 14.** (a) Inventory of dissolvable $CaCO_3$ on the seafloor. Dashed lines represent estimates of the total available inventories of $CaCO_3$. Circles are amounts of seafloor $CaCO_3$ dissolved as a function of fossil fuel $CO_2$ release. (b) The fraction of neutralization of the model by the year 10,000 (circles), determined as the increase in model alkalinity relative to the difference between the initial and the fully neutralized state (calculated as explained in text; results in Table 2). The increase in ocean alkalinity in the year 10,000 (squares) which corresponds to the decrease in erodible layer $CaCO_3$ inventory relative to the initial condition. The bold line would be the result of dissolving the entire 1800 Gt C erodible inventory of $CaCO_3$ on the seafloor (maximum neutralization). Figure 14 shows that (1) seafloor neutralization accounts for most of the ocean alkalinity increase before year 10,000, but (2) seafloor $CaCO_3$ is unable to neutralize the entire net terrestrial $CO_2$ release, even when the $CO_2$ release is smaller than the "potentially erodible" $CaCO_3$ inventory. The reason for this limitation is explained in the text and in Figure 13.

iteration [*Archer*, 1990] as the model chemistry spun up over 1000 years. The resulting inventory of $CaCO_3$ was tallied and plotted against the corresponding value of deep Pacific $[CO_3^=]$, to make up the steady lysocline line in Figure 13a. Below the steady lysocline line, the inventory of $CaCO_3$ is smaller than the steady state value, implying that $\partial$ erodible $CaCO_3$ / $\partial t > 0$. Above, the erodible $CaCO_3$ is declining.

The global steady state of the model balances input of $[CO_3^=]$ to the ocean from continental weathering against removal by $CaCO_3$ accumulation on the seafloor (equation 1). This condition was also found by acceleration. For each of the steady lysocline experiments described above, after the distribution of $CaCO_3$ was calculated at some value of deep Pacific $[CO_3^=]$, the concentration of $[CO_3^=]$ was increased iteratively over a relaxation time of 1000 years, until the global accumulation rate balanced the weathering rate. In contrast to local lysocline equilibrium, the weathering equal accumulation steady state is a global condition, and for this reason this state will be referred to as global throughput steady state. For any value of the $CaCO_3$ inventory there is a corresponding value of ocean $[CO_3^=]$ at which global throughput steady state will obtain, so that global throughput steady state also describes a line on the deep Pacific $[CO_3^=]$ / bioturbated layer $CaCO_3$ phase plot (Figure 13b). The trend of this line is toward increasing deep Pacific $[CO_3^=]$ with increasing bioturbated $CaCO_3$ inventory (a positive slope). This is a somewhat counterintuitive result; one might have expected that more $CaCO_3$ on the seafloor would tend to increase $CaCO_3$ accumulation, requiring a lower $[CO_3^=]$ to compensate. The observed behavior of the model can be understood as follows. The steady state requires that input from weathering, which is held constant in the model, balance the rain of $CaCO_3$ to the seafloor, which is also held constant, minus seafloor $CaCO_3$ dissolution, which is predicted by the model. Throughput balance is therefore determined entirely by the dissolution flux, which increases with increasing $CaCO_3$ inventory on the seafloor. As the $CaCO_3$ inventory increases, a higher value of $[CO_3^=]$ (lesser undersaturation) is required to maintain the requisite dissolution flux. The steady throughput line exhibits positive slope as does the steady lysocline line, but a much steeper slope. The steady throughput line describes the state $\partial[CO_3^=]/\partial t = 0$; area to the left of the line has a positive growth, and area to the right has negative growth.

The division of the phase plane (Figure 13c) into four quadrants determines the behavior of the dynamical system shown in Figure 12. The signs of $\partial/\partial t$ for both state variables of the system are indicated in Figure 13. In region "A," the sediment inventory tends to decrease while the ocean $[CO_3^=]$ tends to increase. The opposite situation is found in region "C." In this region, a transfer of carbon between the sediment and the ocean will act to satisfy the requirements of both reservoirs; the evolution of both reservoirs are "complementary" to each other. In the case of excess dissolution (region A), we have already named this response seafloor neutralization. The response time of seafloor neutralization is relatively fast because the accumulation rate, the middle arrow in Figure 12, is limited only by the kinetics of $CaCO_3$ diagenesis. The weathering rate is held fixed and constant, and burial, the flux of $CaCO_3$ across the erodible line, is by definition nonnegative. In contrast, the accumulation rate flux is free to exceed weathering or to reach negative values. Seafloor neutralization can be envisioned as an internal transfer of $CO_3^=$ within the ocean / sediment system, unbounded by the weathering and burial fluxes.

In the "uncomplementary" regions of the phase space, regions "B" and "D," both the ocean and the sediment evolve in the same direction; in the case of fossil fuel neutralization, both await replenishment by the excess of weathering over burial (terrestrial neutralization). In this regime, the steady accumulation flux can be no greater than the weathering influx nor smaller than the burial flux (which is limited to nonnegative values). The accumulation flux is therefore less dynamic in this case than it was when the model was in one of the complementary regions of the phase plot (A or C). Seafloor $CaCO_3$ no longer contributes to the neutralization of fossil fuel $CO_2$. For this reason, model evolution in this regime is slower than in the complementary regimes. The

transition of the model into the uncomplementary regime at around the year 10,000 is the reason for the increase in *e*-folding timescale for $CaCO_3$ burial after this time in Figure 9b. By 10,000, the alkalinity of the ocean has increased to 60-75% of its final (fully neutralized) value (Figure 14). Most of this increase corresponds to the decrease in erodible $CaCO_3$ inventory on the seafloor, leaving only a small role for terrestrial $CaCO_3$ through this time.

The directions of model evolution in the complementary quadrants in phase space tends to drive the model toward the uncomplementary regions, which serve as dynamical attractors for the model state (Figure 13c). This is demonstrated by the model trajectories in Figure 13d. Once the model reaches one of the uncomplementary regions, it slowly evolves back to the model starting point (the full steady state condition). As it does so, it veers to the left, toward the steady throughput line, indicating that the model achieves steady throughput (nearly steady ocean $[CO_3^{=}]$) while the lysocline lags behind.

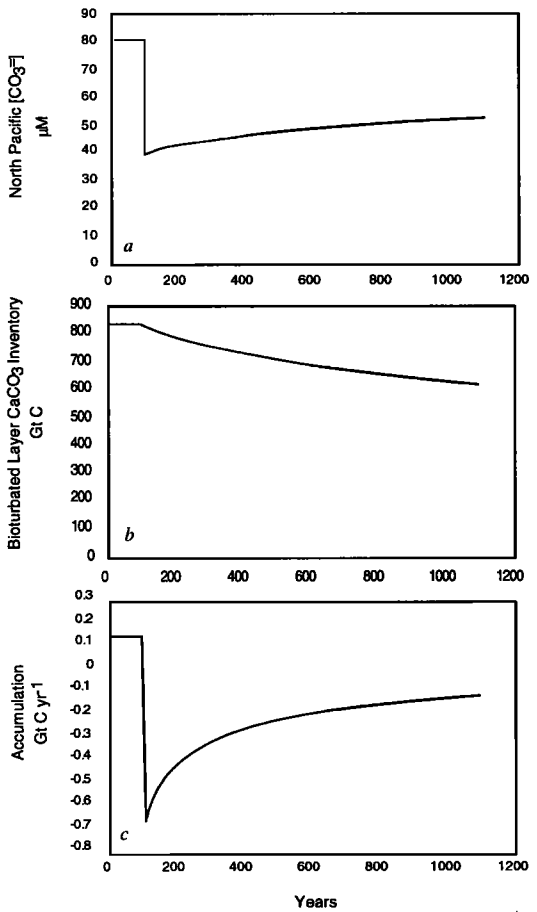


**Figure 15.** The results of adding 100 μM $CO_2$, homogeneously, to the water column of the model, in year 100 of the simulation: (a) time trace of deep Pacific $[CO_3^{=}]$, (b) bioturbated $CaCO_3$ inventory, and (c) model $CaCO_3$ accumulation rate. The accumulation rate "spikes" immediately following the acidification and decreases thereafter to a steady value. It appears that the decreasing dissolution flux over the next 1000 years is not simply a product of changes in deep Pacific $[CO_3^{=}]$ (Figure 15a) or bioturbated layer $CaCO_3$ (Figure 15b).

Table 3. Results of the Dissolution Flux Parameterization Experiments

| Deep Pacific $[CO_3^{=}]$, μmol $L^{-1}$ | Bioturbated Layer $CaCO_3$ Inventory, Gt C | Global $CaCO_3$ Burial Rate, Gt C $yr^{-1}$ |
|---|---|---|
| 86.4 | 1298 | 0.113 |
| 79.1 | 1244 | 0.031 |
| 72.0 | 1187 | -0.053 |
| 65.2 | 1130 | -0.135 |
| 58.8 | 1072 | -0.215 |
| 52.6 | 1015 | -0.289 |
| 47.0 | 958 | -0.359 |
| 87.0 | 834 | 0.144 |
| 78.4 | 763 | 0.073 |
| 70.2 | 699 | 0.000 |
| 60.3 | 662 | -0.053 |
| 52.7 | 613 | -0.109 |
| 45.8 | 565 | -0.161 |
| 39.5 | 522 | -0.205 |
| 85.3 | 440 | 0.170 |
| 76.5 | 382 | 0.099 |
| 67.1 | 330 | 0.049 |
| 58.5 | 318 | 0.011 |
| 50.2 | 284 | -0.028 |
| 42.9 | 252 | -0.061 |
| 36.3 | 225 | -0.087 |
| 85.0 | 245 | 0.178 |
| 75.7 | 185 | 0.117 |
| 66.1 | 135 | 0.068 |
| 58.8 | 139 | 0.043 |
| 50.1 | 117 | 0.017 |
| 42.3 | 102 | 0.000 |
| 35.6 | 90 | -0.015 |

Ocean $[CO_3^{=}]$ and seafloor $CaCO_3$ inventories were perturbed independently of each other. The steady model $CaCO_3$ accumulation rate is taken to be the flux 1100 years after the perturbation as a function of the $[CO_3^{=}]$ and $CaCO_3$ values at that time.

The relationship of model behavior with the two equilibrium conditions is summarized in Plate 2, which relates the global accumulation rate of $CaCO_3$ to deep ocean $[CO_3^{=}]$ and bioturbated layer $CaCO_3$ inventory in three dimensional space and in three two-dimensional projections. The global throughput equilibrium condition (green cubes) can be seen to satisfy the constraint that accumulation equals weathering, while the local lysocline equilibrium (red spheres) does not satisfy this condition except where it intersects the global throughput equilibrium line. The model trajectories intersect the equilibrium conditions in three-dimensional space, supporting our contention that the equilibrium conditions (which were determined independently of the model trajectories) are relevant to the evolution of the model state. Finally, symmetry of the model evolution is demonstrated by a mirror image B scenario which removed $CO_2$ rather than releasing it, which traces a complementary path to B.

**5.5.3. Control of the $CaCO_3$ Accumulation Rate.** We have seen that the behavior of the model is determined by the rates of addition and removal of $CO_3$ from the ocean and surface sedimentary reservoirs and the response of those rates to the fossil fuel perturbation. In particular, the accumulation flux of $CaCO_3$ on the seafloor dominates the fast seafloor neutralization response in the 5 kyr or so of the model

runs. Previous estimates of the $CaCO_3$ compensation timescale [*Boyle*, 1983; *Broecker and Peng*, 1987; *Sundquist*, 1990a; *Walker and Kasting*, 1992] differed in part because of differences in the presumed sensitivity of the global $CaCO_3$ accumulation rate to ocean acidification. In this section we characterize the global $CaCO_3^=$ accumulation rate of the model as a function of $\Delta CO_3$ and the bioturbated $CaCO_3$ inventory (1) for use in understanding the model results and (2) for use in simpler parameterized models of $CaCO_3$ compensation. Because we are parameterizing the dissolution flux as a function of deep Pacific $[CO_3^=]$ and bioturbated layer $CaCO_3$, we refer to these as the parametric model experiments.

The $CaCO_3$ distribution on the seafloor ought to resemble a natural model state, so we adjusted the bioturbated $CaCO_3$ inventory of the model by adjusting the water column $[CO_3^=]$ (a homogeneous perturbation of water column total $CO_2$), spinning up, and then calculating the steady state $CaCO_3$ distribution. Following this, we again perturbed the water column $[CO_3^=]$. A sample result from one of these model experiments (the standard distribution of $CaCO_3$ and a homogeneous addition of 100 μM $CO_2$) is shown in Figure 15. During spin-up, $[CO_3^=]$ increases somewhat and the bioturbated layer $CaCO_3$ inventory decreases, as the model begins to neutralize the added $CO_2$. Dissolution intensity reaches an intense maximum (a minimum in $CaCO_3$ burial) directly after the $CO_2$ addition and stabilizes at lower values after 1000 years. At this time the model is out of steady state (by design), but the accumulation rate is relatively stable with respect to the current values of $\Delta CO_3$ and $CaCO_3$.

Summarizing results of many such model runs, the steady (1000 year) $CaCO_3$ accumulation rates in Table 3 were empirically fit to yield the equation

$$\begin{aligned}\text{Accumulation} = {} & 3.12542\times10^{-3}\ \text{Gt C yr}^{-1}\ (\mu\text{mol kg}^{-1})^{-1}\times[CO_3^=] \\ & - 8.25096\times10^{-4}\ \text{Gt C yr}^{-1}\ (\text{Gt C})^{-1}\times CaCO_3 \\ & + 9.06625\times10^{-6}\ \text{Gt C yr}^{-1}\ (\text{Gt C}\ \mu\text{mol kg}^{-1})^{-1}\times \\ & [CO_3^=]\times CaCO_3 \\ & - 8.626211\times10^{-2}\ \text{Gt C yr}^{-1}\end{aligned}$$

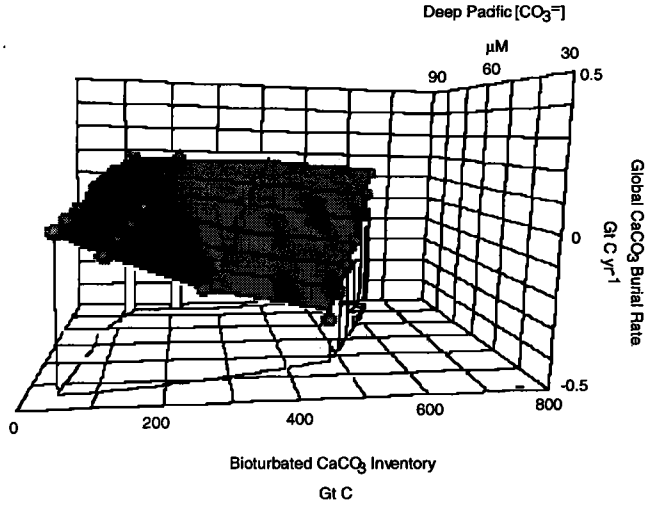


**Figure 16.** Comparison of the steady dissolution flux results from experiments such as shown in Figure 10, with a parameterized empirical function for dissolution as a function of deep Pacific $[CO_3^=]$ and bioturbated layer $CaCO_3$ inventory.

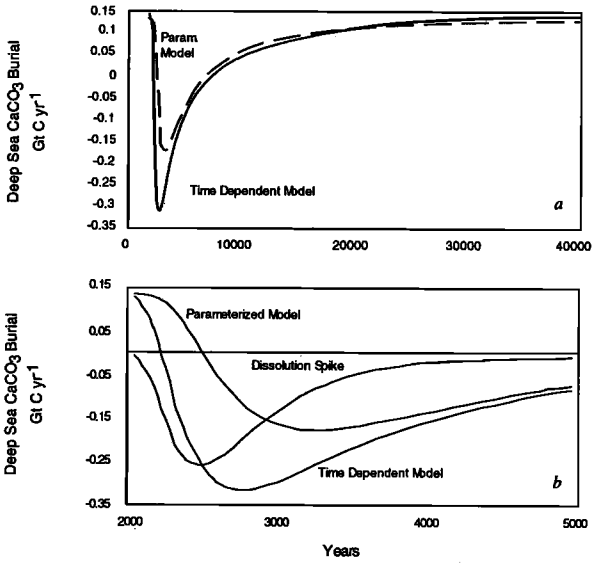


**Figure 17.** (a) A comparison of the full time dependent model results (A22) against predictions of the dissolution flux as a function of the time-evolving values of deep Pacific $[CO_3^=]$ and bioturbated layer $CaCO_3$ inventory. The parameterized function describes the time evolution of the model well, except that it underestimates the magnitude of the time dependent model dissolution flux in the millennium following $CO_2$ release. (b) Detail of the first 5000 years of the experiment with the same comparison as (a) but also showing the dissolution spike, defined as the difference between the time dependent model results and the parameterized function values. The timescale for decay of the dissolution spike resembles the behavior of the model in response to a homogeneous perturbation (Figure 10).

with a fit to the individual model results shown in Figure 16.

The accumulation fluxes expected from the model evolution of $\Delta CO_3$ and bioturbated $CaCO_3$ inventory are compared with the actual model values in Figure 17. It can be seen that the empirically predicted accumulation rate corresponds well except for a significant spike in dissolution immediately following the fossil fuel invasion. Similar behavior was observed in the parametric model runs, a simple example of which was shown in Figure 16. The magnitude of the transitional dissolution spike was calculated by subtracting the model accumulation rate from the empirical prediction, in Figure 17(b). Both the magnitude and the decay time of the transient dissolution spike correspond well to the initial spike of dissolution from the model run in Figure 15.

This observation motivates a closer inspection of the transient behavior of the parametric model run in Figure 15. Over 1000 years following the homogeneous addition of $CO_2$, the dissolution flux decreased more than can be explained by the changing values of $\Delta CO_3^=$ or bioturbated $CaCO_3$ inventory. This behavior was caused by a rearrangement of the distribution of $\Delta CO_3^=$ in the water column, by a process analogous to the formation of a whole ocean boundary layer, caused by surface / deep fractionation of alkalinity in the ocean analogous to the biological pump. The global production rate of $CaCO_3$ in the model is approximately 1.6 Gt C $yr^{-1}$. Most of this $CaCO_3$ redissolves in the water column or at the

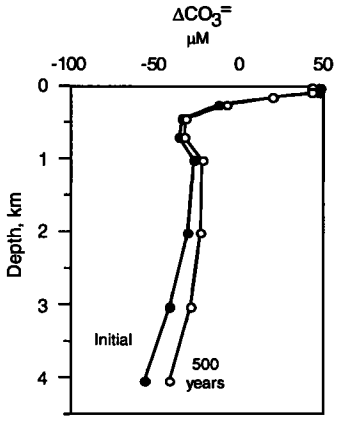


**Figure 18.** A comparison of profiles of $\Delta CO_3^=$ immediately following and 500 years after a homogeneous addition of $CO_2$ to the water column, from 120°E, 0°N.

seafloor, concentrating alkalinity in the deep waters. The dissolution flux from the sediments reached 0.5 Gt C $yr^{-1}$, which acts as an added source of alkalinity to the deep waters comparable to the flux attributable to the biological pump. Over the course of the 1000 year circulation time of the ocean, the alkalinity of deep waters increased until a balance between dissolution and deep ocean circulation was reached. This relaxation is analogous to the formation of a whole ocean boundary layer. Profiles of ocean alkalinity during the dissolution spike and 500 years later are shown in Figure 18. The largest $[CO_3^=]$ changes are found immediately above high $\%CaCO_3$ areas on the seafloor. In the IPCC model runs, the transient dissolution spike is responsible for 50% of the dissolution flux to year 3000 and roughly 10% of the flux to the year 40,000. This transient dissolution spike is the only case where the approximation of the ocean carbonate system as representable by two simple variables, deep Pacific $[CO_3^=]$ and bioturbated layer $CaCO_3$ inventory, breaks down.

## 6. Summary

According to our current understanding, $CO_2$ uptake by rock cycles of the Earth will be slow, with no significant impact on the $pCO_2$ of the atmosphere for the next thousand years. The net terrestrial emission calculated to meet an IPCC atmospheric stabilization scenario (s750) is only a few percent higher when $CaCO_3$ is included in the model simulation, which is negligible compared with uncertainties in biospheric uptake or other aspects of the ocean carbon cycle. Direct ocean injection experiments demonstrate a coupling between dissolution and ocean circulation, as $CaCO_3$ dissolution proceeds somewhat more rapidly for atmospheric and Atlantic injection cases than for Pacific injection. However, $CaCO_3$ dissolution will play only a minor role in determining the fate of fossil fuel $CO_2$ in the coming millennium.

On longer timescales, neutralization of fossil fuel $CO_2$ by the oceans and by $CaCO_3$ takes place in five stages. (1) Invasion of fossil fuel into the oceans will sequester 70-80% of the net terrestrial $CO_2$ release on an $e$-folding timescale of 200-450 years depending on the magnitude of the fossil fuel release. (2) A fast seafloor dissolution spike after $CO_2$ dissolves in the oceans but before alkalinity has a chance to reorganize accounts for half of the neutralization in the coming millennium and 10% of the total $CaCO_3$ dissolution in response to fossil fuel $CO_2$. Beginning in this stage, mankind will have reversed the sedimentation rate of the ocean by dissolving $CaCO_3$ faster than it is deposited on the seafloor; this is projected to peak by the year A.D. 3000 and last up to 5000 years. (3) Steady seafloor dissolution continues until the lysocline reaches local equilibrium with the water column saturation state by about the year A.D. 10,000. Seafloor neutralization overall accounts for 60-70% of the fossil fuel $CO_2$, and has an $e$-folding timescale of 5-6 kyr. (4) Terrestrial weathering replenishes ocean $[CO_3^=]$ on a timescale of 8 kyr after A.D. 10,000 and restores the lysocline to its original depth on a timescale of 18 kyr. Completion of this stage leaves 7-8% of the fossil fuel $CO_2$ remaining in the atmosphere in a new local and global $CaCO_3$ steady state. (5) Neutralization by the silicate rock cycle (not included in the model) restores atmospheric $CO_2$ to some unknown "set point", at which metamorphic decarbonation balances silicate weathering, with a time constant of several hundred thousand years.

**Acknowledgments.** This paper benefitted by reviews by Eric Sundquist, Scott Doney, and another anonymous reviewer, and was supported by the Petroleum Research Fund and the David and Lucille Packard Foundation.

## References

Archer, D. E., The dissolution of calcite in deep sea sediments: An in situ microelectrode study, Ph.D. thesis, Univ. Wash., Seattle, 1990.

Archer, D., Modeling the calcite lysocline, *J. Geophys. Res., 96,* 17,037-17,050, 1991.

Archer, D., An atlas of the distribution of calcium carbonate in sediments of the deep sea, *Global Biogeochem. Cycles, 10,* 159-174, 1996a.

Archer, D., A data-driven model of the global calcite lysocline, *Global Biogeochem. Cycles, 10,* 511-526, 1996b.

Archer, D., S. Emerson, and C. Reimers, Dissolution of calcite in deep-sea sediments: $pH$ and $O_2$ microelectrode results, *Geochim. Cosmochim. Acta, 53,* 2831-2846, 1989.

Archer, D., H. Kheshgi, and E. Maier-Reimer, Multiple timescales for neutralization of fossil fuel $CO_2$, *Geophys. Res. Lett., 24,* 405-408, 1997.

Bacastow, R. B., and R. K. Dewey, Effectiveness of $CO_2$ sequestration in the post-industrial ocean, *Energy Conversi. and Manage., 37,* 1079-1086, 1996.

Berelson, W. M., D. E. Hammond, and G. A. Cutter, In situ measurements of calcium carbonate dissolution rates in deep sea sediments, *Geochim. Cosmochim. Acta, 54,* 3013-3020, 1990.

Berner, E. K., and R. A. Berner, *The Global Water Cycle.*, Prentice-Hall, Englewood Cliffs, N. J., 1987.

Berner, R. A., and J. W. Morse, Dissolution kinetics of calcium carbonate in sea water, IV, Theory of calcite dissolution, *Am. J. Sci., 274,* 107-134, 1974.

Berner, R. A., A. C. Lasaga, and R. M. Garrels, The carbonate-silicate geochemical cycle and its effect on atmospheric carbon dioxide over the past 100 million years, *Am. J. Sci., 283,* 641-683, 1983.

Boyle, E. A., Chemical accumulation variations under the Peru Current during the past 130,000 years, *J. Geophys. Res., 88,* 7667-7680, 1983.

Broecker, W. S., and T. H. Peng, The role of $CaCO_3$ compensation in the glacial to interglacial atmospheric CO2 change, *Global Biogeochem. Cycles, 1,* 15-29, 1987.

Broecker, W. S., and T. Takahashi, Neutralization of fossil fuel $CO_2$ by marine calcium carbonate, in *The Fate of Fossil Fuel* $CO_2$ *in the*

*Oceans*, edited by N. R. Andersen, and A. Malahoff, pp. 213-248, Plenum, New York, 1978.

Cai, W.-J., In situ microelectrode studies of the early diagenesis of organic carbon and $CaCO_3$ in hemipelagic sediments of the Pacific Ocean, Ph.D. thesis, Univ. Calif., San Diego, 1992.

Cias, P., P. P. Tans, M. Trolier, J. W. C. White, and R. J. Francey, A large northern hemisphere terrestrial $CO_2$ sink indicated by the $^{13}C/^{12}C$ ratio of atmospheric $CO_2$, *Science, 269,* 1098-1102, 1995.

Cole, K. H., G. R. Stegen, and D. Spencer, The capacity of the deep oceans to absorb carbon dioxide, *Energy Conv. and Manage., 34,* 991-998, 1993.

Cole, K. H., G. R. Stegen, and D. Spencer, The capacity of the deep oceans to absorb carbon dioxide, in *Direct Ocean Disposal of Carbon Dioxide*, edited by N. Handa, and T. Ohsumi, pp. 143-152, Terra Sci., Tokyo, 1995.

Enting, I. G., T. M. L. Wigley, and M. Heimann (Eds.), Future emissions and concentrations of carbon dioxide: Key ocean/atmosphere/land analyses, 120 pp., Commw. Sci. and Ind. Res. Organ., Melbourne, Victoria, Australia, 1994.

Hales, B., Calcite dissolution on the seafloor: An in situ study, Ph.D. thesis Univ. Wash., Seattle, 1995.

Hales, B., S. Emerson, and D. Archer, Respiration and dissolution in the sediments of the western North Atlantic: Estimates from models of in situ microelectrode measurements of porewater oxygen and pH, *Deep Sea Res., 41 Part I,* 695-719, 1993.

Haugan, P. M., and H. Drange, Disposal options in view of ocean circulation, in *Direct Ocean Disposal of Carbon Dioxide*, edited by N. Handa and T. Ohsumi, pp. 123-141, Terra Sci., Tokyo, 1995.

Hoffert, M. I., Y.-C. Wey, A. J. Callegari, and W. S. Broecker, Atmospheric response to deep-sea injections of fossil-fuel carbon dioxide, *Clim. Change, 2,* 53-68, 1979.

Houghton, J. T., G. J. Jenkins, and J. J. Ephraums (Eds.), *Intergovernmental Panel on Climate Change: The IPCC Scientific Assessment*, Cambridge Univ. Press, New York, 1990.

Houghton, J. T., B. A. Callander, and S. K. Varney (Eds.), *Intergovernmental Panel on Climate Change Climate Change 1992: The Supplimentary Report to the IPCC Scientific Assessment*, Cambridge Univ. Press, New York, 1992.

Houghton, J. T., L. G. Meiro Filho, B. A. Callendar, N. Harris, A. Kattenburg, and K. Maskell (Eds.), *The IPCC Second Scientific Assessment Report*, 572 pp., Cambridge Univ. Press, New York, 1996.

Jahnke, R. A., The global ocean flux of particulate organic carbon: areal distribution and magnitude, *Global Biogeochem. Cycles, 10,* 71-88, 1996.

Jain, A. K., H. S. Kheshgi, and D. J. Wuebbles, A globally aggregated reconstruction of cycles of carbon and its isotopes, *Tellus Ser B 48:* 583-600, 1996.

Keeling, R. F., S. C. Piper, and M. Heimann, Global and hemispheric $CO_2$ sinks deduced from changes in atmospheric $O_2$ concentration, *Nature, 381,* 218-221, 1996.

Keir, R. S., The dissolution kinetics of biogenic calcium carbonates in seawater, *Geochim. Cosmochim. Acta, 44,* 241-252, 1980.

Kheshgi, H. S., B. P. Flannery, M. I. Hoffert, and A. G. Lapenis, The effectiveness of marine $CO_2$ disposal, *Energy, 19,* 967-974, 1994.

Kheshgi, H. S., A. K. Jain, and D. J. Wuebbles, Accounting for the missing carbon sink with the $CO_2$ fertilization effect, *Clim. Change, 33,* 31-62, 1996.

Maier-Reimer, E., The biological pump in the greenhouse, *Global Planet. Change, 8,* 13-15, 1993a.

Maier-Reimer, E., Geochemical cycles in an ocean general circulation model. Preindusrial tracer distributions, *Global Biogeochem. Cycles, 7,* 645-678, 1993b.

Maier-Reimer, E., and K. Hasselmann, Transport and storage of $CO_2$ in the ocean: An inorganic ocean-circulation carbon cycle model, *Clim. Dyn., 2,* 63-90, 1987.

Manabe, S., and R. J. Stouffer, Century-scale effects of increased atmospheric $CO_2$ on the ocean-atmosphere system, *Nature, 364,* 215-218, 1993.

Marchetti, L., On geoengineering the $CO_2$ problem, *Clim. Change, 1,* 59-68, 1977.

Marland, G., R. J. Andres, and T. A. Boden, Global, regional, and national $CO_2$ emissions, in *Trends 93: A Compendium of Data on Global Change*, edited by T. A. Boden et al., Rep. ORNL/CDIAC-65, pp. 505-584, Oak Ridge Nat. Lab., Oak Ridge, Tenn., 1993.

Martin, J. H., G. A. Knauer, D. M. Karl, and W. M. Broenkow, VERTEX: Carbon cycling in the northeast Pacific, *Deep Sea Res. Part A, 34,* 267-285, 1987.

Milliman, J. D., Production and accumulation of calcium carbonate in the ocean: Budget of a nonsteady state, *Global Biogeochem. Cycles, 7,* 927-957, 1993.

Morse, J., and F. T. MacKenzie, *Geochemistry of Sedimentary Carbonates*. Elsevier, New York, 1990.

Nihous, G. C., S. M. Masutani, L. A. Vega, and C. M. Kinoshita, Projected impact of deep ocean carbon dioxide discharge on atmospheric $CO_2$ concentrations, *Clim. Change, 27,* 225-244, 1994.

Panel on Policy Implications of Greenhouse Warming (National Academy of Sciences, National Academy of Engineering, and Institute of Medicine), *Policy Implications of Greenhouse Warming: Mitigation, Adaptation, and the Science Base*, Nat. Acad. Press, Washington, D. C., 1992.

Sarmiento, J. L., J. C. Orr, and U. Siegenthaler, A perturbation simulation of $CO_2$ uptake in an ocean general circulation model, *J. Geophysi. Res., 97,* 3621-3645, 1992.

Schimel, D., I. Enting, M. Heimann, T. Wigley, D. Raynaud, D. Alves, and U. Siegenthaler, $CO_2$ and the carbon cycle, in *Climate Change 1994: Radiative Forcing of Climate Change and an Evaluation of the IPCC IS92 Emission Scenarios*, edited by J. T. Houghton et al., pp. 35-71, Cambridge Univ. Press, New York, 1994.

Sundquist, E. T., Geological perspectives on carbon dioxide and the carbon cycle, in *The Carbon Cycle and Atmospheric $CO_2$: Natural Variations Archean to Present, Geophys. Monogr. Ser.*, vol 32, edited by E. T. Sundquist, and W.S. Broecker, pp. 5-59, AGU, Washington D. C., 1985.

Sundquist, E. T., Geologic analogs: Their value and limitations in carbon dioxide research, in *The Changing Carbon Cycle, A Global Analysis*, edited by J. R. Trabalka and D. E. Reichle, pp. 371-402, Springer-Verlag, New York, 1986.

Sundquist, E. T., Influence of deep-sea benthic processes on atmospheric $CO_2$, *Philos. Trans. R. Soc. London Ser. A, 331,* 155-165, 1990a.

Sundquist, E. T., Long-term aspects of future atmospheric $CO_2$ and sea-level changes, in *Sea-Level Change*, edited by R. Revelle, pp. 193-207, Nat. Acad. Press, Washington, D. C., 1990b.

Tans, P. P., I. Y. Fung, and T. Takahashi, Observational constraints on the global atmospheric $CO_2$ budget, *Science, 247,* 1431-1438, 1990.

Tsunogai, S., and S. Noriki, Particulate fluxes of carbonate and organic carbon in the ocean. Is the marine biological activity working as a sink of the atmospheric carbon?, *Tellus Ser. B, 43,* 256-266, 1991.

Walker, J. C. G., and J. F. Kasting, Effects of fuel and forest conservation on future levels of atmospheric carbon dioxide, *Palaeogeog., Palaeoclimatol., Palaeoecol., 97,* 151-189, 1992.

Walker, J. C. G., P. B. Hays, and J. F. Kasting, A negative feedback mechamism for the long-term stabilization of Earth's surface temperature, *J. Geophys. Res., 86,* 9776-9782, 1981.

Wigley, T. M. L., R. Richels, and J. A. Edmonds, Economic and environmental choices in the stabilization of $CO_2$ concentrations: Choosing the "right" emissions pathway, *Nature, 379,* 240-243, 1996.

Wolery, R. J., and N. H. Sleep, Interactions of geochemical cycles with the Mantle, in *Chemical Cycles in the Evolution of the Earth*, edited by C. B. Gregor et al., pp. 77-104, John Wiley, New York, 1988.

D.E. Archer, Department of the Geophysical Sciences, University of Chicago, 5734 South Ellis Avenue, Chicago, IL 60637. (e-mail: d-archer@uchicago.edu)

H. Kheshgi, Exxon Research and Engineering Company, Route 22E, Annandale, NJ 08801 (email hskhesh@erenj.com)

E. Maier-Reimer, Max-Plank-Institut fuer Meteorologie, Bundesstrasse 7, D-2000 Hamburg 54, Germany (email maier-reimer@dkrz.de)

(Received January 24, 1998; revised February 2, 1998; accepted February 25, 1998.)